PNC ZA 0995 96-001
UCB-NE-4218

Underground Autocatalytic Criticality from Fissile Materials Solidified in Borosilicate Glass

J. Ahn, S. Armel, J. Burch, P. L. Chambré, E. Greenspan, and D. A. Roberts

Department of Nuclear Engineering
University of California
Berkeley, California 94720

August 1997

The authors invite comments and would appreciate being notified of any errors in the report.

Joonhong Ahn
Department of Nuclear Engineering
University of California
Berkeley, CA 94720
USA

ahn@nuc.berkeley.edu

Table of Contents

List of Figures

List of Tables

Acknowledgments

The research reported herein was supported by the Isolation System Research Program, Radioactive Waste Management Program, Power Reactor and Nuclear Fuel Development Corporation, Japan, under contract PNC ZA 0995 96-001 .

1. INTRODUCTION AND BACKGROUND

1.1 Scope of This Study

Bowman and Venneri [1] postulated scenarios for large energy releases from fissile materials buried in geologic repositories by autocatalytic criticality (see Section 1.2 for its definition). Their primary interest was the possibility of autocatalytic criticality related to the weapons-grade plutonium (w-Pu) and highly-enriched uranium (HEU) to be disposed of in the proposed Yucca Mountain repository. The geologic formation hosting the repository is characterized as a fractured volcanic tuff with partial saturation with water. An independent scenario study has been done at the Nuclear Engineering Department, University of California at Berkeley (UCB) [2–4].

In the study reported on herein, an independent assessment of the feasibility of the autocatalytic criticality phenomena is conducted for the case with vitrified high-level wastes (HLW) from reprocessed fuel of commercial light-water reactors. Although no specific repository site or host rock type has been announced for vitrified HLW disposal, it is assumed in this study that the HLW is to be disposed of in fractured granitic rock saturated with water, as is assumed in the Japanese [5] or Swiss [6] HLW geologic disposal projects.

To investigate the possibility of the autocatalytic criticality scenario for the vitrified HLW disposed of in a repository hosted by a water-saturated granitic rock, we address the following two questions, which have not been addressed either in the Japanese or Swiss HLW geologic disposal project, or in the Bowman and Venneri's study:

"In the geologic, hydrologic and geochemical settings that were considered in the previous performance assessment studies for vitrified HLW disposal, what is the theoretical maximum mass of thermally fissile materials (TFM) that can accumulate downstream from the repository?" and,

"Are there any geometric and material configurations consisting of TFM and water-saturated granite which are critical and can exhibit positive reactivity feedback?"

To help answer these questions, the present study consists of the following tasks:

Chapter 2

The repository configurations and the geologic formation hosting the repository, which are assumed in this study, are summarized, by adopting assumptions in [5].

Chapter 3

Because the total mass of TFM and their decay precursors in a single canister of HLW is far less than a minimum critical mass (Section 1.4), a sufficient amount of TFM contributed by multiple canisters must be accumulated for criticality.

We establish a mathematical model for release, transport and accumulation of TFM, to obtain theoretical worst-case predictions for TFM accumulation in the assumed geologic, hydrologic and geochemical settings [5]. We have made a number of conservative assumptions, where reliable quantitative data are not available because the repository site is not known as yet.

Chapter 4

Even if TFM may accumulate in significant amounts, without positive feedback mechanisms for neutron multiplication driven by fission energy release, the criticality is not characterized as autocatalytic, and so energy release by the criticality event will be insignificant. Neutronics analyses for various mixtures of TFM and water-saturated rock have been performed.

1.2 Criticality Phenomena in Geologic Formations

1.2.1 Autocatalytic Criticality

Fissile energy release could, in principal, occur if chemical and hydrologic processes reconfigure TFM into a configuration, where the effective multiplication factor[1] k_{eff} exceeds unity and increases with fissile energy release. Rock and water slow (moderate) fast neutrons to thermal velocities by collisions with light nuclei, facilitating fission of the thermally fissile isotopes ^{235}U, ^{233}U and ^{239}Pu. Thus, the fission power will climb with time as

$$P = P_o e^{\alpha t} \tag{1.1}$$

where the inverse period or "time eigenvalue" α is equal to

$$\alpha = \frac{k_{eff} - 1}{\Lambda} \tag{1.2}$$

with Λ being the effective neutron generation time. See **Figure 1.1**. We define here autocatalytic criticality as criticality with positive reactivity[2] feedback with fissile energy release, or with increase in the system temperature. In all autocatalytic critical systems, the energy release eventually terminates after negative feedback mechanisms force α to become negative.

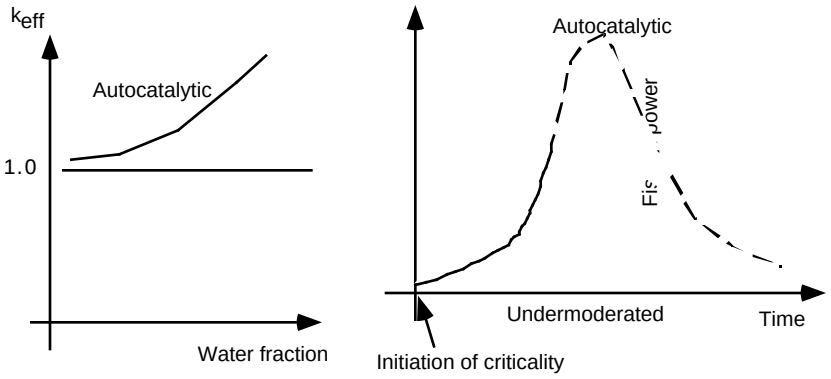

Figure 1.1 Concept of autocatalytic criticality. In the left figure, the effective multiplication factor increases with temperature increase. The solid curve in the right figure depicts the initial increase in energy release represented by Eq. (1.1).

1.2.2 Undermoderated Dry Criticality at a Waste Emplacement

Bowman and Venneri [1] proposed a scenario called undermoderated (dry) autocatalytic criticality occurring at the original emplacement of weapons plutonium immobilized in borosilicate glass, in intimate contact with surrounding fractured rock. The scenario required that the stronger neutron absorbers, such as boron, leach out from the glass before significant ^{239}Pu decay occurs, leaving plutonium behind. Subsequently the resulting undermoderated

---

[1] *Effective multiplication factor*

The multiplication factor is defined as the ratio of the number of fissions in any one generation to the number of fissions in the immediately preceding generation. The effective multiplication factor characterizes the neutron multiplication in a finite system, out of which neutrons leak with a certain probability.

[2] *Reactivity* is defined as $\rho = \frac{k_{eff} - 1}{k_{eff}}$.

configuration was assumed to be driven critical by dispersion of the plutonium into surrounding rock, effectively adding more moderator (i.e., rock matrix) to the initially undermoderated system and thus increasing reactivity. They then postulated that vaporized plutonium would vent through fractures in the surrounding dry rock, providing a positive reactivity feedback mechanism.

While previous reviews have confirmed the neutronics calculations performed by Bowman and Venneri, none have supported their views for the formation of critical deposits or energy release [7–10]. Likelihood of undermoderated autocatalytic criticality can be made vanishingly small by engineering design of waste package, poisons, and near field, such as adding neutron absorbers with solubilities comparable to that of plutonium [2–4].

1.2.3 Over-moderation and Under-moderation with Water

Water absorbs neutrons more effectively than many types of rock. Hence, in a geologic setting, a system is overmoderated when the neutron-absorbing effect of water exceeds its moderating contribution, so that water expulsion from rock pores increases reactivity (the left figure of **Figure 1.2**).

The overmoderated, subcritical system could become supercritical either by accumulation of more TFM to the system or by water expulsion from the system. For instance, uranium deposition below the water table could become critical if the water table drops, as might occur with ground-water pumping. The initial heating would expel water even further. Then, there could be two cases:

- If the system has positive reactivity feedback mechanisms driven by system temperature increase other than water removal, then the system enters the autocatalytic criticality regime.
- Otherwise, water will continue to be expelled, and the system eventually enters the undermoderated regime. The power generated by the fission chain reactions then levels off and remains roughly constant at a level just sufficient to compensate for the heat transferred to the outside regions. This phenomenon is considered to have happened at the Oklo natural reactor about two billion years ago [11].

Overmoderated criticality in a geologic setting was recognized in the late 1970s, but generated less interest at that time because no plans existed to dispose of HEU and it was difficult to postulate credible chemical mechanisms to separate plutonium from the large quantities of neutron-absorbing ^{238}U in commercial spent fuel [12, 13]. Bowman and Venneri proposed scenarios of overmoderated autocatalytic criticality [1] for TFM depositions occurring in the host rock via transport of TFM from the multiple canisters to depositions.

The UCB study [2–4] for the autocatalytic criticality with w-Pu and HEU in the Yucca Mountain settings shows that:

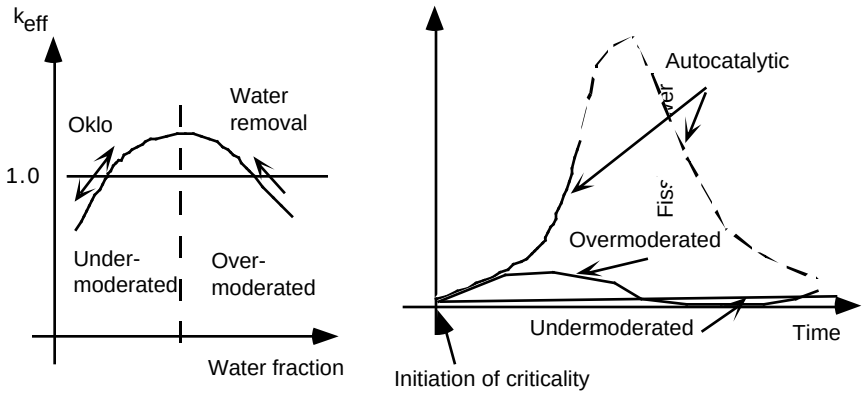

Figure 1.2 Over-moderation and under-moderation.

- Pu-rock-water systems can be autocatalytic. Spectrum hardening due to the rock temperature increase has been identified as a positive reactivity feedback mechanism, because of the existence of the 0.3 eV resonance peak of ^{239}Pu. Other mechanisms such as water expulsion and the homogenization of heterogeneous deposition of Pu in moist rock by some physical mechanisms have also been identified as positive feedback mechanisms for reactivity.
- Heterogeneous HEU-rock-water systems might become autocatalytic. Spectrum hardening due to the rock temperature increase has been identified as a positive reactivity feedback mechanism, because of the reduction in the spatial self-shielding by the TFM depositions (see Chapter 4 for more details), and
- At Yucca Mountain, it is highly unlikely that Pu will travel large distances to form these configurations. Plutonium 239 will decay to ^{235}U before most of a glass waste form is leached. Uranium 235 can move large distances as a solute, however it is unlikely to precipitate into these critical configurations due to lack of reducing agents.

1.3 Natural Uranium Deposition and Autocatalytic Criticality

Natural uranium ore deposits provide evidence for the configurations uranium might take, if it were to precipitate away from a repository. For example, in the Peña Blanca uranium deposit in Mexico, pitchblende (UO_{2+x}) is found in fault zones in fractured tuff as coatings, veinlets, stringers and disseminations. In deposits of this type, average uranium weight fractions can be 0.3 percent, reaching 10 percent locally [14].

Figure 1.3 shows that these weight fractions would be sufficient to reach criticality in infinite, homogeneous systems, where the neutron multiplication factor, k_∞ is maintained unity, for uranium with enrichment greater than roughly 4%. For finite systems, neutron leakage increases the critical weight fraction of uranium somewhat.

Heterogeneity can greatly increase the weight fraction of uranium to achieve criticality. For uranium deposited in parallel fractures spaced at 20 cm rather than homogeneously, **Figure 1.3** shows that the critical weight fraction doubles or quadruples depending on water content. Increasing water content in the rock matrix, like heterogeneity, increases the weight fraction of

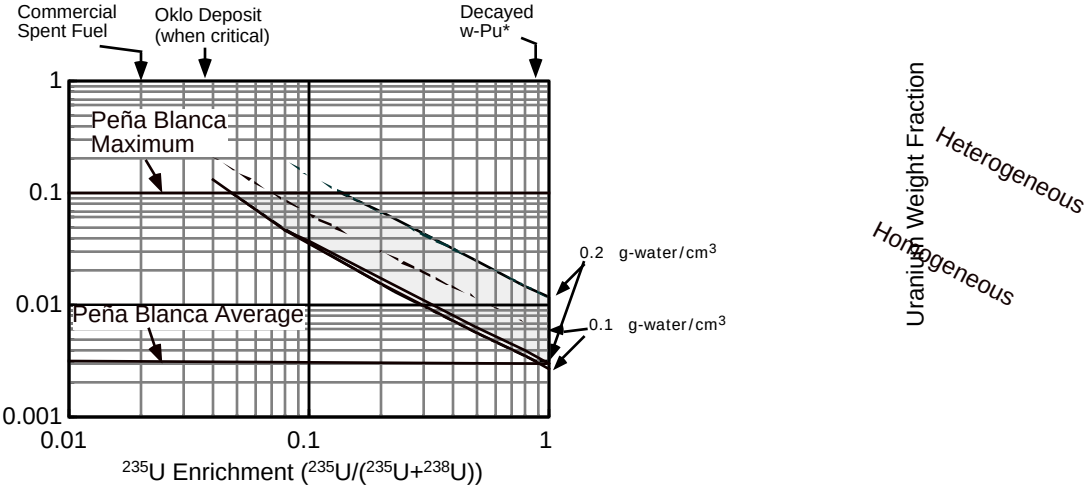

Figure 1.3 Average uranium fraction required to achieve criticality, $k_\infty = 1$, in tuff rock (2.2 g/cm^3) [2]. Homogeneous mixtures (solid curves) require lower weight fractions than heterogeneous UO_{2+x} coatings in parallel fractures spaced at 20 cm (dashed curves). (*Approximate enrichment, diluted primarily with ^{236}U.)

uranium for criticality.

1.4 Assumed High-Level Waste Characteristics

In **Table 1.1**, given are the inventories of (1) radionuclides in 1 MT of spent fuel from PWR initially enriched at 4.5% with a burnup of 45,000 MWD/MT and (2) radionuclides in HLW arising from 1 MT of the same spent fuel. The spent fuel is stored for four years of cooling before reprocessing. At reprocessing, it is assumed that 99.33% of plutonium and 99.85% of uranium are recovered. It is assumed that HLW from 1 MT of PWR spent fuel is vitrified with borosilicate glass and contained in one waste canister. The vitrified HLW is stored for fifty years before emplacement in the repository. The waste glass is assumed to start radionuclide release a thousand years after the emplacement. The origin of the time axis (t = 0) is placed at the moment when radionuclide release from glass logs begins, i.e., 1054 years after the discharge of spent fuel from a reactor.

Table 1.1 Radionuclides Contained in One HLW Glass Log Generated From Reprocessing of 1 MT of Spent Fuel, at the Beginning of Radionuclide Release From the Glass Log.

	Nuclide	2200 m/sec cross section [15]		Half-life	Inventory			
		fission	absorption		HLW		Spent fuel	
		[barn]		[yr]	[mol]	[kg]	[mol]	[kg]
	Pu-240	———	289.5	6.57E+3	2.0E-1	4.8E-2	3.0E+1	7.2
	U-236	———	5.2	2.34E+7	5.6E-2	1.3E-2	3.7E+1	8.8
√	Cm-245	2020	345	9.30E+3	7.6E-3	1.8E-3	7.6E-3	1.8E-3
	Am-241	3.15	916	4.58E+2	2.8E-1	6.8E-2	2.8E-1	6.8E-2
	Np-237	0.02	169	2.14E+6	4.0	0 95	4.0	0 95
√	U-233	531.1	47.7	1.62E+5	1.2E-3	2.9E-4	8.2E-1	1.9E-1
	Pu-242	<0.2	18.5	3.76E+5	1.8E-2	4.4E-3	2.7	6.5E-1
	U-238	———	2.70	4.46E+9	5.8	1.4	3.9E+3	9.3E+1
	U-234	———	100.2	2.45E+5	1.1E-2	2.6E-3	7.4	1.7
	Am-243	———	154.5	7.37E+3	4.9E-1	1.2E-1	4.9E-1	1.2E-1
√	Pu-239	742.5	268.8	2.44E+4	2.5E-1	6.1E-2	3.8E+1	9.1
√	U-235	582.2	98.6	7.04E+8	7.0E-2	1.6E-2	4.7E+1	1.1E+1
	B	———	759	———	1.0E+3	5.7E+1	———	———

99.85% of U and 99.33% of Pu are assumed to be recovered at the reprocessing stage. Calculated by ORIGEN2 code [16]. B_2O_3 content is assumed to be 14 wt%. Total weight of borosilicate glass is assumed to be 405 kg. Notice that inventories for Cm, Am, and Np isotopes in HLW are the same those in spent fuel. Nuclides with √ mark are fissile; others are categorized as neutron absorbers (or poisons).

Because of relatively small mass of fissile materials and large mass of boron in each glass log, the possibility of the undermoderated dry criticality at a waste emplacement would be null provided that boron and other poisons are not "washed". The HLW canister in **Table 1.1** contains around 0.06 kg of ^{239}Pu and 0.05 kg of ^{240}Pu. This is far below the minimum critical mass. For example, Sanchez *et al.* [17] calculated the minimum critical mass of ^{239}Pu uniformly and homogeneously distributed over reflected spherical cores made of either water, silica or tuff rock to be, respectively, 0.49 kg, 35.1 kg, or 85.6 kg.

However, minor actinides, such as ^{245}Cm, ^{241}Am, ^{237}Np, and ^{243}Am, which will not be recovered by reprocessing, and residual ^{242}Pu, ^{240}Pu and ^{239}Pu decay to uranium isotopes. For example, after a sufficiently long time, ^{243}Am and ^{239}Pu will decay to ^{235}U. With the inventories given in **Table 1.1**, the maximum mass of ^{235}U available is calculated as 0.486 + 0.254 + 0.07 = 0.810 mol. Similarly, 0.00755 + 0.282 + 4.02 + 0.00124 = 4.31 mol for ^{233}U, 0.018 + 5.83 = 5.85 mol for ^{238}U, 0.2 + 0.0559 = 0.26 mol for ^{236}U are obtained. With these numbers, the TFM enrichment, defined as (^{235}U + ^{233}U)/(^{236}U + ^{238}U + ^{235}U + ^{233}U), can be calculated as (0.81 + 4.31)/(0.26 + 5.85 + 0.81 + 4.31) = 46%. If we do not include the contribution by ^{233}U because of its relatively short half-life, the enrichment can be calculated as 12%.

In spent fuel, the amount of ^{238}U is so large that the contribution of minor actinides is negligible. The TFM enrichment for spent fuel is calculated as (85.1 + 5.13)/(67.2 + 3890 + 85.1 + 5.13) = 2.2%. This is the most important difference between spent fuel and vitrified HLW.

Therefore, for overmoderated criticality, there is a possibility of a TFM deposition occurring, which has an enrichment high enough for criticality in the context of **Figure 1.3**, if TFM released from multiple waste glass logs is transported through the engineered barriers and the surrounding host rock by groundwater, and accumulates somewhere in the host rock due to some change in geochemical and hydrological conditions.

1.5 Summary

For weapons-grade plutonium and highly-enriched uranium disposed of at Yucca Mountain proposed repository [2-4], it has been found that there exists positive reactivity feedback with fissile energy release. In the case of HLW, the possibility that such a high enrichment is achieved as in the Yucca Mountain Study is unlikely. However, due to the existence of actinide isotopes in the HLW glass logs, which will eventually decay to uranium isotopes, there is a possibility of creating enrichment greater than that of natural uranium. These sources of uranium are distributed in the tens of thousands of waste canisters in the repository.

Under these circumstances, the aims of this study are the following:

First, although we do not know yet the details of the repository design or characteristics of hosting geologic formations, we conduct radionuclide transport analysis, and estimate the mass of uranium accumulation and its enrichment. Accumulation is assumed to occur in the host rock away from, and contributed by, multiple HLW canisters in the repository. This analysis is done in such a way that it gives an upper bound of the mass of accumulated uranium and its enrichment. If the uranium mass accumulation can be shown likely to be very small, one could close the study at this point.

But, if one can identify the case where the possibility of uranium accumulation of relatively high enrichment is achieved, then one must proceed to the neutronics analysis. Here, we estimate the mass of accumulated uranium required for overmoderated criticality in granite with the enrichment obtained in the transport analysis. We compare it with the total mass of actinides originally available in the repository. If it is too large, again, we can close the study at this point.

If the mass for overmoderated criticality is still of concern, we will proceed to the analysis for positive feedback mechanisms. Possible positive feedback mechanisms in geologic formations have already been pointed out in [2-4]. We consider whether the same positive feedback mechanisms are also possible for the assumed configuration of the uranium accumulation obtained by the transport analysis. If the neutronics analysis gives no positive feedback mechanisms, then we can also conclude that the autocatalytic criticality is highly unlikely for the case with vitrified HLW.

2. GEOLOGIC FORMATIONS AND REPOSITORY CONFIGURATION

2.1 Geologic Formations Hosting Repository

The type of a rock hosting a repository may affect the criticality scenario in two ways: first, the transport of fissile and poison materials in the host rock, and, second, required critical mass and its neutronic characteristics. Because the host rock type for a future Japanese repository has not yet been determined, we herein determine representative geologic formations, by reviewing the previous performance assessment study [5].

The geological units of the Japan archipelago are grouped into the following five categories:

1.Paleozoic-Paleogene strata,
2.Granitic rocks and rhyolitic rocks,
3.Neogene strata,
4.Quaternary sediments, and
5.Quaternary volcanic rocks.

The main rocks composing these categories are summarized in **Table 2.1**

Table 2.1 Major types of rocks composing in Japan [5]

	Major constituent rocks		Hydrogeological characteristics
	Igneous/Pyroclastic rock	Sedimentary rock	
Paleozoic-Paleogene strata	basalt, ultrabasic rock,	clastic rocks of sandstone and mudstone, chert, limestone,	fractured
Granitic rocks and rhyolitic rocks	granite, rhyolite		fractured
Neogene strata	andesite, basalt, dacitic pyroclastic rock	mudstone,	porous
Quaternary sediments		gravel, sand, mud, along with volcanic materials	porous
Quaternary volcanic rocks	lava, pyroclastic sediments, pyroclastic fall deposits, tuff		fractured/porous

From a global perspective, the percentage of igneous rock that can be found on the earth's surface is not so large. However, the Japan archipelago is an exception; in particular, the percentage of igneous rocks in and after the Cretaceous period is quite large. In this study, we choose igneous rock as a representative host rock for a repository.

Igneous rocks are classified by their chemical composition and texture. Igneous rocks with SiO_2 fraction greater than 66% are called acidic rock or felsic rock. Those with SiO_2 fractions between 52% and 66%, 45% and 52%, and less than 45% are called intermediate rock, basic rock, and ultrabasic rock, respectively. Basalt and andesite are examples of basic and intermediate rocks, respectively. Granite, dacite, and rhyolite are categorized as felsic rock. Typical composition of granite is tabulated in **Table 2.2**. The composition is similar to that of Yucca Mountain tuff.

Table 2.2 Reference granite composition [18].

Oxide	Weight %	Oxide	Weight %
SiO_2	69.17	MgO	1.15
TiO_2	0.39	CaO	3.15
Al_2O_3	15.00	Na_2O	3.45
FeO	2.48	K_2O	3.01
Fe_2O_3	1.05	P_2O_5	0.13
MnO	0.10		

In **Table 2.3**, neutron cross-sections for some naturally occurring elements are tabulated. With **Table 2.2** and **Table 2.3**, it is pointed out that the minimum critical mass in pure silica is expected to be smaller than in granite (see Chapter 4).

Table 2.3 2200 m/sec cross sections for naturally occurring elements [19]

Element	σ_a (barn)	σ_s (barn)	σ_t (barn)
H_2O	0.66	103	103
B	755	4	759
O	0.0002	4.2	4.2
Na	0.525	4	4.53
Mg	0.069	3.6	3.67
Al	0.241	1.4	1.64
Si	0.16	1.7	1.86
P	0.20	5	5.20
S	0.52	1.1	1.62
Cl	33.8	16	49.8
K	2.07	1.5	3.57
Ca	0.44	3.0	3.44
Ti	5.8	4	9.8
Mn	13.2	2.3	15.5
Fe	2.62	11	13.6

Hydrologically, igneous rocks can be characterized as fractured or porous media (**Table 2.1**). In either case, a repository will be built under the water table [5]. Therefore, the radionuclide transport analysis can be made under the assumption that any void spaces in the repository and the surrounding host rock are fully saturated with water.

One of the major findings in the UCB study [2–4] on the criticality event at the proposed Yucca Mountain repository is that the important positive feedback mechanism for reactivity stems from the heterogeneity of accumulated fissile material. Therefore, we assume that the geologic formation hosting the repository is characterized as a fractured medium.

2.2 Repository Configuration

Detailed repository design is yet to be determined. **Figure 2.1** is an example of a basic repository layout proposed in [5]. Totally 40,000 waste canisters would be disposed of by placing them horizontally in disposal tunnels at a pitch of 7 m (**Figure 2.2**). The tunnels are spaced 15 m apart. Thus, roughly 100 m^2 is allocated for a waste canister, and the repository has dimensions of 2,000 m × 2,000 m. The repository depth is assumed to be 1,000 m.

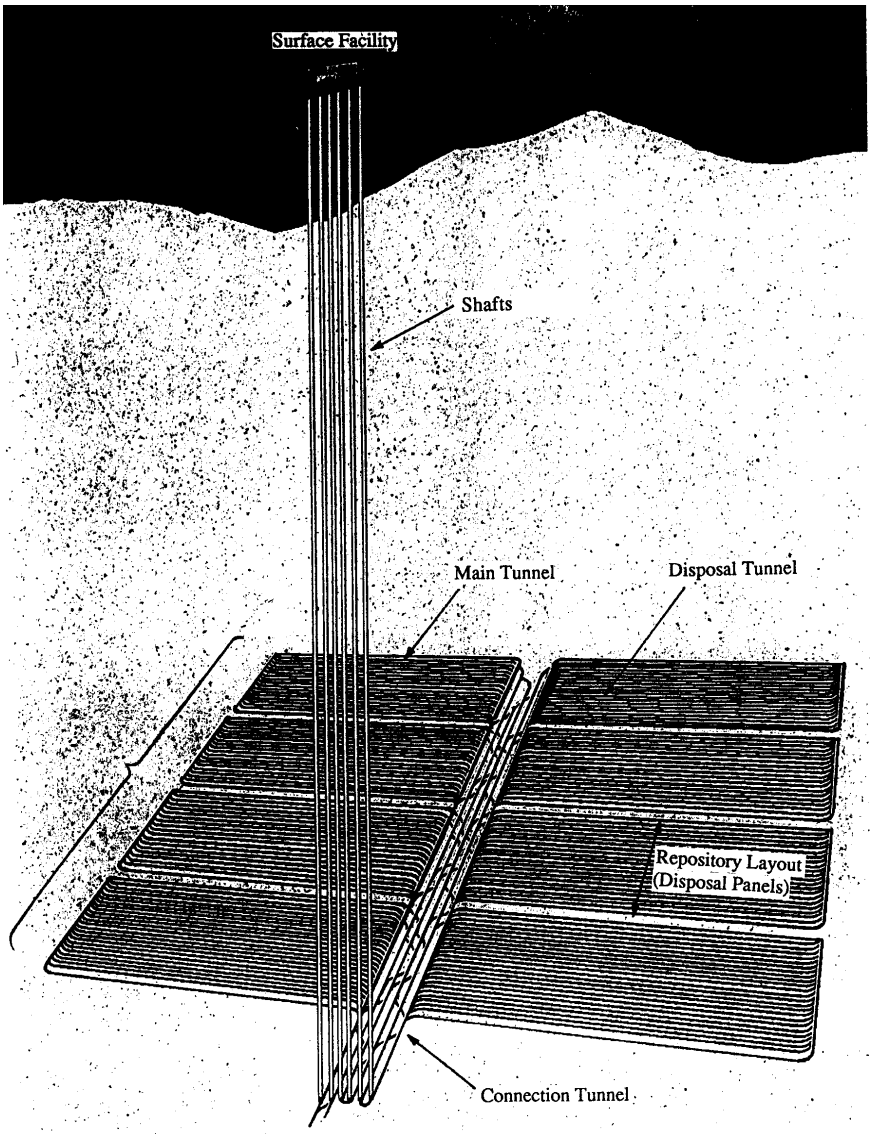

Figure 2.1 A proposed layout of disposal facility [5].

For engineered barriers around the waste canister, a thick carbon-steel overpack and a bentonite-filled buffer region exist between the waste solid and the host rock. The dimensions are given in **Figure 2.2** [5].

The lifetime of an overpack is conservatively estimated as a few thousand years in the disposal condition. In the performance assessment study [5], it was assumed to be 1,000 years. In early stage of this period (the first 1,000 years after the emplacement of the waste canister), the heat generation from a canister would rapidly decrease, and the temperature in the repository would settle down to the ambient temperature (~ 50^{o}C). The bentonite buffer would be fully saturated by groundwater by then.

Once the overpack loses its integrity, the waste glass starts to dissolve by porewater in the bentonite buffer, together with the fissile and other materials contained in the glass log. Bentonite is expected to have a hydraulic conductivity more than three orders of magnitude smaller than that of the surrounding host rock [5]. Bentonite swells by water uptake, and seals intersecting fractures. Due to pyrite in bentonite and the carbon-steel overpack, the porewater in

the engineered-barrier region will be in a reducing state. Due to favorable properties of bentonite, the hydrological and geochemical condition within the engineered barriers is assumed constant in time.

Under the stable reducing environment, most actinide elements are hardly soluble. Actinides released from the glass log by alteration of glass matrix will precipitate immediately. The concentrations in the porewater contacting their precipitates are limited by their solubilities.

Actinides will be transported through the porewater in the bentonite buffer region by molecular diffusion. The bentonite will be compacted before it is used as a backfill, and so will function as a filter for colloids. Presence of colloids is neglected in the analysis hereafter; materials are transported as solute.

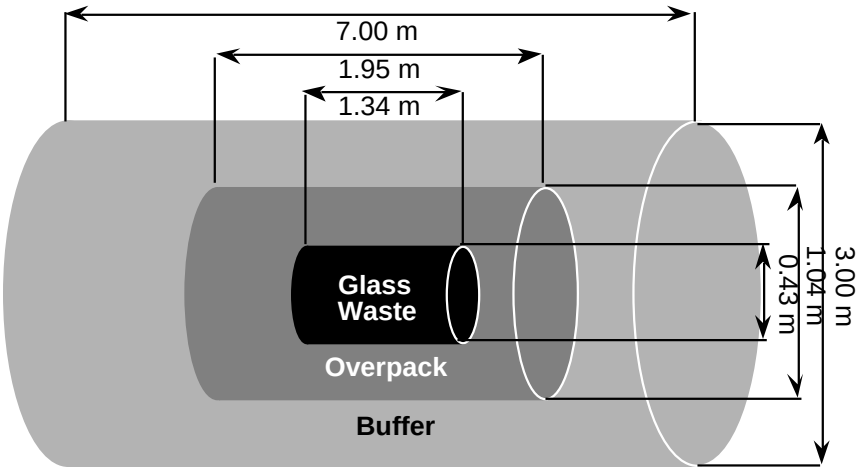

Figure 2.2 Engineered barrier dimensions [5]

3. RELEASE, TRANSPORT, AND ACCUMULATION OF THERMALLY FISSILE MATERIALS

3.1 Scope of This Chapter

The objective of this chapter is to obtain masses of fissile and poison materials accumulated in the surrounding host rock as a function of time and distance from the repository. This information will be utilized in the next chapter, where the neutronics analysis is presented.

The masses of uranium, plutonium, and minor actinides (Am, Cm, and Np) in one HLW glass log are not sufficient to produce a critical configuration at the emplacement location. The possibility for such event to occur requires transport of radionuclides away from the glass logs and their accumulation somewhere in the host rock by geochemical and hydrogeological processes.

Although we need to know the geochemical and hydrogeological mechanisms causing accumulation of uranium in the host rock to quantify the mass of accumulated uranium, the host rock type for the repository is yet to be determined. Therefore, in this study, we aim at obtaining the theoretical upper bound of the accumulated masses without specifying the detailed accumulation mechanisms, but with the following assumptions.

First, it is assumed conservatively that all the radionuclides released from all the glass logs in the repository are transported to a single accumulation location, and deposited there. Thus, the results obtained are hypothetical worst-case estimates, and are applicable for a wide variety of rocks.

Second, it is assumed that each glass log contributes to the accumulation without being influenced by other glass logs. See **Figure 3.1**(a). A mathematical model is developed for the transport and accumulation of radionuclides in the water-saturated geologic formation. This model is coupled with a source term model, which describes how the radionuclides in the glass log are released and transported in the engineered barriers. After we obtain the mass of accumulated radionuclides contributed by a single glass log as a function of time and the transport distance between the glass log and the accumulation location, the total mass of accumulation in the host rock is estimated by superposing all 40,000 glass-log contributions of the repository into a single accumulation.

Because in reality long-lived radionuclides such as uranium released from the upstream glass logs interfere the release of the same species from the downstream glass logs, due to the smaller concentration gradient at the glass log surfaces (see **Figure 3.1**(b)), the model depicted by **Figure 3.1** always gives greater mass accumulation, and is conservative.

In the source term model, solubility limit at the location of waste-solid alteration and the subsequent transport of radionuclides in the engineered barriers are considered. Multiple-member decay chains are taken into account both in the transport model for the geologic formation and in the source term model. For the transport of radionuclides in the geologic formation, the parallel planar fracture model is adopted, for which the analytical solution has been obtained elsewhere [20]. For the source term, new analytical solutions are obtained.

3.2 Mathematical Models

We consider the mass transport between the position of individual glass logs and the accumulation region in the host rock. We assume that the transport path between the two locations is independently set for each glass log, while the accumulation location is shared by all

the glass logs. By this assumption, the mass of accumulated TFM will be conservatively overestimated.

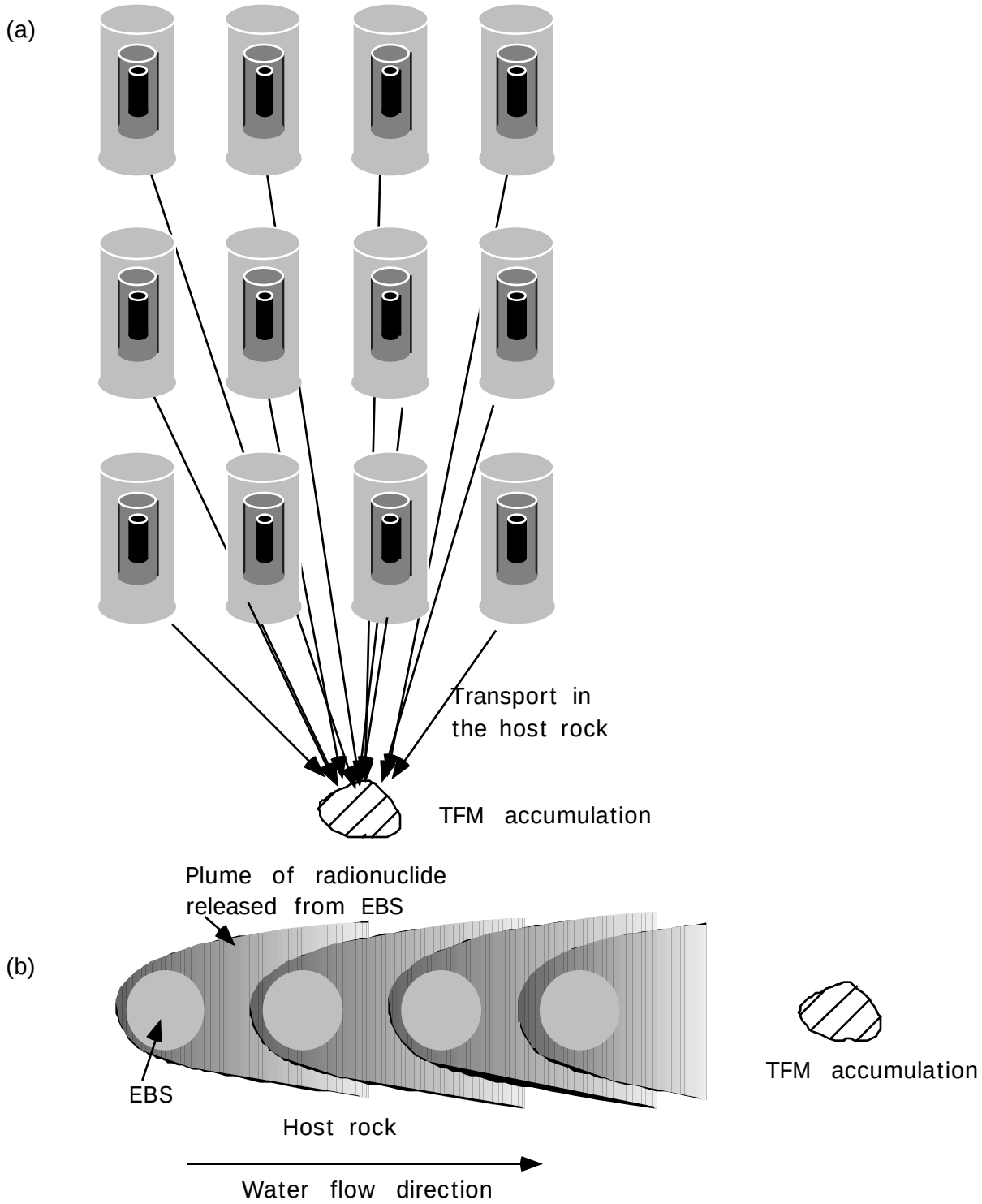

Figure 3.1 (a) Contributions of individual glass logs to the accumulation are treated independently. (b) It is considered that the concentration of a radionuclide released from glass logs in a row increases as water flow through

For the transport and accumulation in the host rock, we adopt the parallel fracture model (Section 3.2.1). For the release of radionuclides into the host rock, we develop a source term model by considering the release of radionuclides from the glass log and the transport in the engineered barrier (Section 3.2.2).

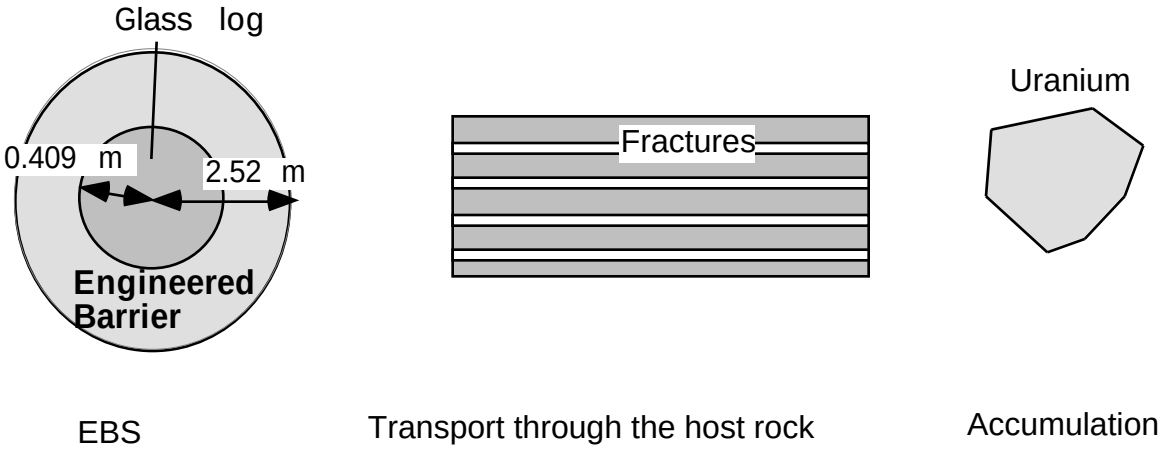

Figure 3.2 Schematic illustration of model structure.

3.2.1 Transport and Accumulation in Host Rock

Consider a rock matrix containing multiple parallel planar fractures of width 2*b*, with a spacing of 2*a*, situated in a water-saturated porous rock of porosity ε_p (See **Figure 3.3**). We include the following physical and chemical phenomena in the model for the radionuclide transport in the natural barrier: (a) advection in the fractures, (b) longitudinal hydrodynamic dispersion in the direction of the axis of the fractures, (c) molecular diffusion in the rock matrix, (d) sorption onto the fracture surfaces, (e) sorption in the rock matrix, and (f) radioactive decay chains of arbitrary length.

The velocity *v* and the longitudinal hydrodynamic dispersion coefficient D^L are assumed to be constant with time and uniform in the fracture. They are also assumed to be common for all radionuclides, since the hydrodynamic dispersion is determined mainly by the geometry of the contaminant transport paths.

Molecular diffusion of radionuclides from water flowing in the fractures into stationary water in the pores of the rock matrix is an important retardation mechanism. In the present study, we use an intrinsic diffusion coefficient, $D^I_{e(k)}$, for radionuclide *k* of element *e* in the rock defined as

$$D^I_{e(k)} = \varepsilon_p \tau_p D^F_{e(k)}. \tag{3.1}$$

where τ is the tortuosity correction factor for the porous host rock, and $D^F_{e(k)}$ the diffusion coefficient in free water. Here, subscript *e(k)* indicates that the *k*-th member nuclide in a decay chain is an isotope of element *e*.

Sorption to the materials filling the fractures and sorption within the rock matrix are considered separately because of the possibility of differing chemical properties in the fracture and the rock matrix. For the porous rock matrix, we define the capacity factor $\alpha_{e(k)}$ for radionuclide *k* of element *e* as

$$\alpha_{e(k)} = \varepsilon_p + \rho_p (1 - \varepsilon_p) K^e_{dp}, \tag{3.2}$$

where ρ [kg/m^3] is the density of the porous rock matrix, and K_{dp}^e [m^3/kg] the sorption distribution coefficient of element *e* for the rock matrix. The retardation coefficient, $R_{e(k)}$, for advection and longitudinal dispersion in the fractures can be defined as

$$R_{e(k)} = 1 + \frac{\rho_f (1 - \varepsilon_f) K_{df}^e}{\varepsilon_f}, \tag{3.3}$$

where ρ_f and ε_f are the density and the porosity of the material filling the fractures. K_{df}^e [m^3/kg] is the sorption distribution coefficient of element *e* for the material filling the fractures.

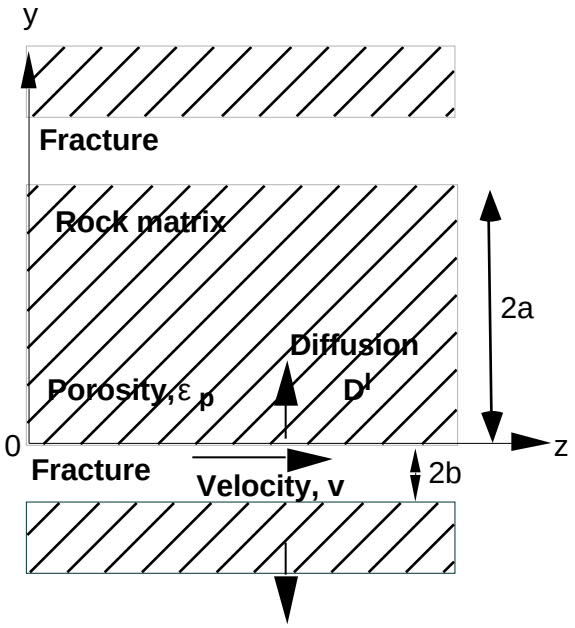

Figure 3.3 Conceptual configuration of parallel fractures in the host rock. Radionuclides released from the engineered barriers enter from the left.

We make the following assumptions relating to the geometry and hydraulic properties of the system [21]. The assumption is made that diffusion and dispersion across the fracture aperture assures complete mixing, and that mass transport along the fracture can be represented as a one-dimensional flow field. Furthermore, it is assumed that the permeability of the porous rock is very low and transport in the rock will be mainly by molecular diffusion, and that the direction of mass flux in the rock matrix is perpendicular to the fracture plane.

We can simplify the basically two-dimensional system into two one-dimensional systems: one for the concentration of radionuclides in water in the fracture and one for their concentration in water in the rock pores. The coupling of two one-dimensional systems is provided by the continuity of fluxes and concentrations along the rock/fracture interface.

3.2.1.1 Accumulation

To estimate accumulation of TFM in the host rock, we make an assumption, which leads to the upper bound, that all the radionuclide of interest arriving at a certain point a distance [illegible] far from the surface of the engineered barrier will precipitate and accumulate there. Then, the governing equation for the mass $\Omega_k(t)$ of the *k*-th radionuclide in a decay chain of length *i*, accumulated at $z =$ [illegible] is written as

$$\frac{d\Omega_k}{dt} = -\lambda_k\Omega_k(t) + \lambda_{k-1}\Omega_{k-1}(t) + S_k(t), t > 0, \text{ subject to } \Omega_k(0) = 0, \quad (3.4)$$

for $k = 1, 2, \ldots, i$, with $\lambda_0 = 0$, where

$$_k(t) = vC_k(t) - D^L\frac{\partial C_k}{\partial z}\bigg|_{z=0}, t > 0 \quad (3.5)$$

is the mass flux of radionuclide k at a distance z from the fracture entrance. D^L is the longitudinal hydrodynamic dispersion coefficient. λ_k [yr^{-1}] is the decay constant of radionuclide k. $C_k(z, t)$ is the concentration of radionuclide k in the fracture, for which the governing equation is given in the next section.

S_f [m^2] is the cross sectional area of the fractures intersecting the repository area per glass log. With the repository dimensions of $L_R \times L_R$ [m^2], the number, n_w, of the glass logs placed in the repository, and the number, n_f, of the fractures intersecting the repository, S_f is expressed as

$$S_f = \frac{2bL_R n_f}{n_w}, \quad (3.6)$$

where we assume that each fracture has a cross-sectional area of $2bL_R$.

3.2.1.2 *Transport in the Host Rock*

The basic radionuclide transport equations for the concentrations $C_k(z, t)$ in the fracture and $C_k^P(y, t; z)$ in the pores of the rock matrix are, respectively,

$$R_{e(k)}\frac{\partial C_k}{\partial t} + v\frac{\partial C_k}{\partial z} - D^L\frac{\partial^2 C_k}{\partial^2 z} - \frac{D^I_{e(k)}}{b}\frac{\partial C_k^P}{\partial y}\bigg|_{y=0} + R_{e(k)}\lambda_k C_k - R_{e(k-1)}\lambda_{k-1}C_{k-1} = 0, \quad t > 0, z > 0, \quad (3.7)$$

and

$$\alpha_{e(k)}\frac{\partial C_k^P}{\partial t} = D^I_{e(k)}\frac{\partial^2 C_k^P}{\partial y^2} - \alpha_{e(k)}\lambda_k C_k^P + \alpha_{e(k-1)}\lambda_{k-1}C_{k-1}^P, t > 0, 0 < y < a, z > 0. \quad (3.8)$$

The initial and boundary conditions are:

$$C_k(z, 0) = 0, z > 0, \quad (3.9)$$

$$C_k^P(y, 0; z) = 0, 0 < y < a, z > 0, \quad (3.10)$$

$$\varepsilon\left[v_I C_k(0, t) - D_I^L\frac{\partial C_k}{\partial z}\bigg|_{z=0}\right] = \frac{Q_k(t)}{A}, t > 0, \quad (3.11)$$

$$C_k(\infty, t) = 0, t > 0, \quad (3.12)$$

$$C_k^P(0, t; z) = C_k(z, t), t > 0, z > 0, \quad (3.13)$$

$$\frac{\partial C_k^P}{\partial y}\bigg|_{y=a} = 0, t > 0, z > 0. \quad (3.14)$$

Some of the parameters are defined in (3.1), (3.2), and (3.3). The constants v_I and D_I^L in (3.11) are set equal to v and D^L, but may be set to other values if required. The time dependent function, $Q_k(t)$, in (3.11) is the flux of radionuclide k from the engineered barrier, and is obtained later by considering the mass transport in the engineered barrier with help of (3.49). The factor A, dimensionless, in (3.11) is expressed as

$$A = \frac{S}{S_2}, \tag{3.15}$$

where S_2 is the surface area of an equivalent spherical EBS (see **Figure 3.4**) containing one glass log. S_f is given by (3.6).

3.2.2 Release from Engineered Barrier

3.2.2.1 Assumptions and Governing Equations

To evaluate the concentration, $C_k(z, t)$, with which the mass flux, $j_k(z, t)$, of radionuclide k is evaluated by (3.5), one needs to determine $Q_k(t)$, the mass flux at the entrance of the fracture. To establish the mathematical model for evaluating $Q_k(t)$, we start with the review of the engineered barriers.

In designs proposed for the HLW repository in water-saturated geologic formations [3], a metal container and a bentonite-filled buffer region exist between the waste solid and the host rock. In the present study, the region between the waste solid and the surrounding rock formation is simplified as a single uniform porous medium, whose physical and chemical properties are represented by those of bentonite. This region is called the bentonite region herein.

Bentonite is expected to have a hydraulic conductivity more than three orders of magnitude smaller than that of the surrounding host rock [5]. Therefore, it is assumed that radionuclides are transported only by molecular diffusion through the stationary water in the pores of the bentonite region. Because molecular diffusion is constrained in tortuous paths in the pores, the diffusion coefficient, $D_{e(k)}$ [m^2/yr], in the bentonite region for element e is smaller than that in free water, $D_{e(k)}$, by the tortuosity correction factor τ.

To simplify, we consider an equivalent sphere for the waste solid and the bentonite region, which has the same interfacial areas (see **Figure 3.4**).

To obtain $Q_k(t)$, therefore, we need to know the concentration, $N_k(r, t)$, of radionuclide k in the water phase in the bentonite region. With $N_k(r, t)$, we can define $Q_k(t)$ as

$$Q_k(t) = -\varepsilon D_{e(k)} \frac{\partial N_k}{\partial r}\bigg|_{r=r_2} \tag{3.16}$$

Here, it is assumed that the diffusive mass transport in the bentonite region has no angular dependency; $Q_k(t)$ is assumed to be uniform on the bentonite/rock interface. By using (3.16) in (3.11), it is further assumed that radionuclides released at the bentonite/rock surface enter the fractures which connect with the accumulation location.

The governing equations for the radionuclide concentrations $N_k(r, t)$ in the EBS are written as

$$\begin{aligned}
K_{e(1)} \frac{\partial N_1}{\partial t} + \lambda_1 K_{e(1)} N_1 &= D_{e(1)} \frac{1}{r^2} \frac{\partial}{\partial r}\left(r^2 \frac{\partial N_1}{\partial r}\right), \\
K_{e(2)} \frac{\partial N_2}{\partial t} + \lambda_2 K_{e(2)} N_2 &= D_{e(2)} \frac{1}{r^2} \frac{\partial}{\partial r}\left(r^2 \frac{\partial N_2}{\partial r}\right) + \lambda_1 K_{e(1)} N_1, \\
&\vdots \qquad\qquad \vdots \\
K_{e(i)} \frac{\partial N_i}{\partial t} + \lambda_i K_{e(i)} N_i &= D_{e(i)} \frac{1}{r^2} \frac{\partial}{\partial r}\left(r^2 \frac{\partial N_i}{\partial r}\right) + \lambda_{i-1} K_{e(i-1)} N_{i-1}, \\
t > 0, \;\; r_1 < r < r_2 &
\end{aligned} \tag{3.17}$$

where r [m] is the distance from the center of the waste solid, t [yr] time, and $K_{e(k)}$ the dimensionless retardation coefficient, for element e in the EBS. Isotopes of element e have identical retardation and diffusion coefficients. r_1 and r_2 [m] are the radii of the equivalent-sphere waste solid and bentonite region, respectively.

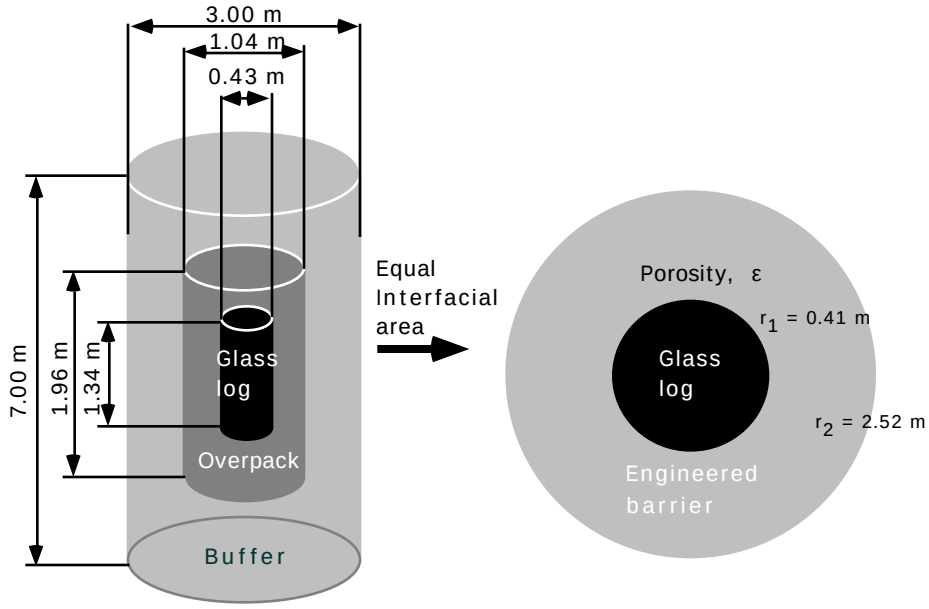

Figure 3.4 Conceptual configuration of the engineered barrier. The dimensions for the original cylindrical geometry are referred from **Figure 2.2**, and apply to a spherical barrier region with corresponding interface areas defined by r_1 and r_2.

We assume that local sorption equilibrium between radionuclide concentrations in the water and in the solid of the bentonite region is established. Sorption is also assumed to be a reversible reaction with a constant distribution coefficient, K_d^e [m^3/kg]. Sorption retards movement of radionuclides by molecular diffusion. The retardation coefficient, $K_{e(k)}$, is defined as:

$$K_{e(k)} = 1 + \frac{\rho(1 - \varepsilon)}{\varepsilon} K_d^e \tag{3.18}$$

where ρ [kg/m^3] and ε are the density and the porosity of the bentonite, respectively. Here, K_d^e is determined for each element e.

3.2.2.2 Side Conditions

The governing equations (3.17) are solved, subject to the following initial and boundary conditions.

There are no radionuclides in the bentonite region initially. Hence, the initial condition is written as

$$N_k(r, 0) = 0, r_1 < r < r_2, \; k = 1, 2, \ldots, i. \tag{3.19}$$

At the outer boundary, $r = r_2$, it is assumed that

$$N_k(r_2, t) = 0, t > 0, \; k = 1, 2, \ldots, i. \tag{3.20}$$

This boundary condition gives a steeper concentration gradient in the bentonite region, resulting in a greater release to the host rock, than reality.

On the waste-solid surface, $r = r_1$, if the solubility of radionuclide k is low compared with the amount of radionuclide k released by the alteration of the waste solid matrix, then all the radionuclides released cannot dissolve into the water phase. We consider two extreme cases that are described below.

In one case, it is assumed that the precipitate of radionuclide k covers the entire waste-solid surface uniformly, and that the precipitate thickness increases or decreases in time. Then, at the waste-solid surface, $r = r_1$,

$$N_k(r_1, t) = \gamma_k(t)\, N_e^* \{h(t) - h(t - t_k^*)\},\ t > 0, k = 1, 2, \ldots, i, \tag{3.21}$$

where $h(\bullet)$ is the Heaviside step function, N_e^* [mol/m^3] the solubility of element e and $\gamma_k(t)$ the fraction of radionuclide k in the precipitate of element e, defined as

$$\gamma_k(t) = \frac{P_k(t)}{\sum P_k(t)},\ k = 1, 2, \ldots, i. \tag{3.22}$$

$P_k(t)$ [mol] is the amount of precipitate k at $r = r_1$ (see (3.26)). The summation in the denominator is taken over all the isotopes of element e. t_k^* [yr] is the time when the precipitate disappears, which can be determined by the analysis shown later in this section.

In the other case, it is assumed that there is no precipitate of radionuclide k at the surface of the waste solid. Then, at $r = r_1$,

$$-D_{e(k)}\varepsilon \frac{\partial N_k}{\partial r}\bigg|_{r=r_1} = m_k(t)\{h(t) - h(t - T_L)\},\ t > 0,\ k = 1, 2, \ldots, i, \tag{3.23}$$

where $m_k(t)$ [mol/m^2·yr] is the congruent release rate of radionuclide k (see (3.31)). T_L [yr] is the leach time of the waste solid, which is the time period between the beginning and the end of the waste solid alteration.

The boundary conditions, (3.21) and (3.23), can be symbolically represented by

$$-(1 - \sigma_k)D_{e(k)}\varepsilon \frac{\partial N_k}{\partial r}\bigg|_{r=r_1} + \sigma_k N_k(r_1, t) = \begin{cases} \gamma_k(t)\, N_e^* \{h(t) - h(t - t_k^*)\}, & \text{for } \sigma_k = 1 \\ m_k(t)\{h(t) - h(t - T_L)\}, & \text{for } \sigma_k = 0 \end{cases} \quad t > 0,\ k = 1, 2, \ldots, i \tag{3.24}$$

where σ_k is a constant whose value is either 1 or 0, corresponding to the boundary conditions (3.21) and (3.23), respectively. Hereafter, we denote symbolically the right-hand side of (3.24) as $\psi_k(t)$:

$$\psi_k(t) = (1 - \sigma_k)m_k(t)\{h(t) - h(t - T_L)\} + \sigma_k \gamma_k(t)\, N_e^* \{h(t) - h(t - t_k^*)\},\ t > 0,\ k = 1, 2, \ldots, i, \tag{3.25}$$

In summary we solve the governing equations (3.17) subject to the initial condition (3.19) and the boundary conditions (3.20) and (3.24).

3.2.2.3 Determination of Inner Boundary Conditions

The amount, $P_k(t)$, of precipitate k is governed by

$$\frac{dP_k}{dt} = \begin{cases} S\{m_k(t) - q_k(t)\} - \lambda_k P_k + \lambda_{k-1} P_{k-1}, & 0 < t < T_L, \\ -Sq_k(t) - \lambda_k P_k + \lambda_{k-1} P_{k-1}, & t > T_L, \end{cases} \quad \text{subject to } P_k(0) = 0,\ k = 1, 2, \ldots, i, \tag{3.26}$$

where $S = 4\pi r_1^2$ [cm^2] is the surface area of the waste solid. The analytical expressions for $q_k(t)$ and $m_k(t)$ are obtained below.

The amount of the precipitate will change by dissolution into the water phase and by radioactive decay. The dissolved radionuclide will diffuse away from the precipitate. The rate, $q_k(t)$, of removal of radionuclide k from the precipitate by molecular diffusion at $r = r_1$ is defined as

$$q_k(t) = -\varepsilon D_{e(k)} \left. \frac{\partial N_k}{\partial r} \right|_{r=r_1}, \; t > 0, \; k = 1, 2, \ldots, i. \tag{3.27}$$

$N_k(r, t)$ is the solution obtained by solving (3.17) subject to the initial condition (3.19), the boundary condition (3.20), and the solubility-limited boundary condition,

$$N_k(r_1, t) = \gamma_k(t) N^*_{e(k)}, \; t > 0, \; k = 1, 2, \ldots, i, \tag{3.28}$$

instead of (3.21). The analytical solution has been obtained elsewhere [22], from which the diffusive mass flux, $q_k(t)$, can be derived as

$$q_k(t) = \varepsilon D_{e(k)} \varphi_k(t) \left\{ \frac{1}{r_1} + \sqrt{\nabla_k} \coth\left(\sqrt{\nabla_k} L \right) \right\} + \frac{2\varepsilon D_{e(k)}}{L} \sum_{m=1}^{\infty} \alpha_m \left(\frac{\varphi_k(t)}{\delta_k} - \int_0^t \exp\left(-\delta_k (t - \tau) \right) \varphi_k(\tau) d\tau \right)$$

$$- \frac{2\varepsilon D_{e(k)}}{L} \sum_{j=1}^{k-1} \left[\frac{D_{e(j)}}{K_{e(k)}} \left\{ \prod_{n=j}^{k-1} \lambda_n \right\} \sum_{n=j}^{k} \frac{\sum_{m=1}^{\infty} \beta_m^2 \int_0^t \exp\left(-\delta_n (t - \tau) \right) \varphi_j(\tau) d\tau}{\prod_{\substack{n=j \\ n \neq j}}^{k} \left(\delta_n - \delta_j \right)} \right], \; t > 0, \; k = 1, 2, \ldots, i, \tag{3.29}$$

where $\nabla_k = \dfrac{K_{e(k)} \lambda_k}{D_{e(k)}}$, $L = r_2 - r_1$, $\alpha_m = \beta_m^2 \dfrac{K_{e(k)}}{D_{e(k)}}$, $\delta_k = \lambda_k + \alpha_m$, $\beta_m = \dfrac{m\pi}{L}$, $\varphi_k(t) = \gamma_k(t) N^*_{e(k)}$,

$$k = 1, 2, \ldots, i. \tag{3.30}$$

The amount of the precipitate increases due to the radioactive decay of the precursor and the release of radionuclide k by alteration of the waste solid. If we assume that the glass alters at a constant rate during the leach time T_L, the congruent release rate, $m_k(t)$, is obtained by solving:

$$\frac{dm_k}{dt} = -\lambda_k m_k + \lambda_{k-1} m_{k-1}, \; 0 < t < T_L, \; k = 1, 2, \ldots, i, \; \lambda_0 = 0, \tag{3.31}$$

subject to $m_k(0) = m_k^o$, where m_k^o [mol/m^2·yr] is defined as

$$m_k^o = \frac{M_k^o}{S T_L}, \; k = 1, 2, \ldots, i, \tag{3.32}$$

and M_k^o [mol] is the inventory of radionuclide k in the waste solid at the beginning of the waste-solid alteration. (3.31) is mathematically equivalent to the Bateman equations, whose solutions are readily available [15] as

$$m_k(t) = m_k^o e^{-\lambda_k t} + \sum_{j=1}^{k-1} \left[m_j^o \left\{ \prod_{i=j}^{k-1} \lambda_i \right\} \left\{ \sum_{i=j}^{k} \frac{\exp\left(-\lambda_i t \right)}{\prod_{\substack{n=j \\ n \neq i}}^{k} \left(\lambda_n - \lambda_i \right)} \right\} \right], 0 \le t \le T_L, \; k = 1, 2, \ldots, i. \tag{3.33}$$

With (3.29) and (3.33), the solution to (3.26) is obtained as

$$P_k(t) = F_k(t) \quad \exp(-\lambda_k t) + \sum_{i=1}^{k-1} \left\{ \prod_{n=1}^{k-1} \lambda_n \right\} F_i(t) \quad \sum_{n=i}^{k} \frac{\exp(-\lambda_n t)}{\prod_{\substack{j=i \\ j \neq n}}^{k} (\lambda_j - \lambda_n)}, \; 0 \le t \le T_L, \; k = 1, 2, \ldots, i, \qquad (3.34)$$

where $(f * g)(t) \equiv \int_0^t f(\tau) g(t-\tau) d\tau$, $F_k(t) = S\left[m_k(t) \{ h(t) - h(t - T_L) \} - q_k(t) \right]$, $k = 1, 2, \ldots, i$. (3.35)

To evaluate $\gamma_k(t)$ exactly based on the definition (3.22), one has to know N_k. Thus, the problems must be solved iteratively. To decouple the precipitation analysis from the radionuclide diffusion analysis for the bentonite region, we approximate the definition of $\gamma_k(t)$ as

$$\gamma_k \approx \frac{\int_0^{T_L} m_k(t) dt}{\sum_e \int_0^{T_L} m_k(t) dt}, \; k = 1, 2, \ldots, i. \qquad (3.36)$$

Notice that γ_k in (3.22) is replaced by its integral overage by utilizing the analytical solution for $m_k(t)$ given by (3.33). This approximation is good for long-lived radionuclides such as uranium isotopes. However, if the radionuclide has a smaller initial inventory than its precursor and the solubility is relatively large, then the precipitate will not be created until sufficient accumulation is achieved in the waste solid due to the decay of the precursor. This could occur for the case of the ^{243}Am —> ^{239}Pu —> chain.

$P_k(t)$ is initially zero by the initial condition. $P_k(t)$ increases with time at early times if more radionuclide k is released from the glass log by alteration of the glass matrix than diffuses away from the precipitate (refer to the right-hand side of eq. (3.26)). Eventually $P_k(t)$ starts to decrease because the congruent release rate decreases or even becomes zero after the leach time while the diffusive mass flux stays nearly constant as long as the precipitate exists there. Finally, $P_k(t)$ becomes zero at some time t_k^*. Thus, for this case, a positive t_k^* is obtained by solving $P_k(t_k^*) = 0$, and the precipitate k exists until the time, t_k^*, and the boundary condition (3.21) applies.

If the solubility is high enough, or the half-life of the radionuclide is short enough, the right-hand side of (3.26) becomes negative shortly after $t = 0$, and so $P_k(t) < 0$ (no precipitation occurs) for $t > 0$. For this case, no positive t_k^* is obtained by solving $P_k(t_k^*) = 0$, and the congruent-release boundary condition (3.23) applies.

Precipitation can occur not only at the interface ($r = r_1$) but also in the bentonite region, if the precursor has a greater retardation coefficient, a greater solubility and a shorter half-life. In the present analysis, we neglect precipitation of radionuclides within the bentonite region, based on the result of the previous analysis for diffusion of a ^{241}Am –> ^{237}Np decay chain [23]. This analysis shows that precipitation in the bentonite region has minor effects on the mass release rate at the bentonite/rock interface, and that the effects become even smaller if the lifetime of the metal canister is longer than 6000 years.

3.3 Analytical Solutions

From (3.4), the Laplace transform for the mass of TFM, $\Omega_k(t)$, is obtained as

$$\tilde{\Omega}_k = S \sum_{i=1}^{k} \left[\frac{\tilde{\psi}_i(\tilde{t}; s)}{\lambda_k} \prod_{p=i}^{k} \frac{\lambda_p}{s+\lambda_p} \right], \quad k = 1, 2, \ldots, i, \tag{3.37}$$

where s is a complex Laplace variable. The tilde ~ symbol stands for a Laplace-transformed function. The Laplace-transformed mass flux, $\tilde{\psi}_k(\tilde{t}; s)$, of radionuclide k at a distance $\tilde{t}$ from the fracture entrance is by the Laplace transform of (3.5) as

$$\tilde{\psi}_k(\tilde{t}; s) = v\tilde{C}_k(\tilde{t}; s) - D^L \frac{d\tilde{C}_k}{dz}\bigg|_{z=1}, \quad k = 1, 2, \ldots, i. \tag{3.38}$$

The Laplace-transformed analytical solution, $\tilde{C}_k(z; s)$, has been obtained elsewhere [20]. If we set $v_I = v$ and $D_I^L = D^L$ in that solution and substitute the resultant into (3.38), we obtain

$$\tilde{\psi}_k(\tilde{t}; s) = \sum_{m=1}^{k} \sum_{n=1}^{m} u_{mk}(s) v_{nm}(s) \exp\left[-b_m(s)z\right] \frac{\tilde{Q}_n(s)}{\varepsilon A_f}, \quad k = 1, 2, \ldots, i \tag{3.39}$$

where

$$\zeta_m(s) = \sqrt{\frac{(s+\lambda_m)\alpha_{e(m)}}{D^I_{e(m)}}}, \tag{3.40}$$

$$b_m(s) = \frac{v}{2D^L}\left\{-1 + \sqrt{1 + \frac{4D^L g_m(s)}{v^2}}\right\}, \tag{3.41}$$

$$g_m(s) = R_{e(m)}(s+\lambda_m) + \frac{D^I_{e(m)}}{b}\zeta_m(s)\tanh\left[\zeta_m(s)a\right], \tag{3.42}$$

$$\left[g_k(s) - g_m(s)\right]u_{mk}(s) = R_{e(k-1)}\lambda_{k-1}u_{m,k-1}(s) + \sum_{n=m}^{k-1} B_{nk}(s)u_{mn}(s), \tag{3.43}$$

with

$$u_{kk}(s) = 1, \tag{3.44}$$

$$B_{nk}(s) = -\frac{D^I_{e(k)}}{b}\left(\prod_{l=n}^{k-1} \frac{\alpha_{e(l)}\lambda_l}{D^I_{e(l+1)}}\right)\sum_{l=n}^{k} \frac{\zeta_l(s)\tanh\left[\zeta_l(s)a\right]}{\prod_{\substack{j=n \\ j\neq l}}^{k}\left[\zeta_j^2(s) - \zeta_l^2(s)\right]}, \tag{3.45}$$

$$a_m(s) = \frac{1}{v_I + D_I^L b_m(s)} \sum_{n=1}^{m} v_{nm}(s)\frac{\tilde{Q}_n(s)}{\varepsilon A_f}, \tag{3.46}$$

and

$$v_{nm}(s) = -\sum_{j=n}^{m-1} u_{jm}(s)v_{nj}(s) \qquad \text{for } m > n \tag{3.47}$$

with

$$v_{mm}(s) = 1. \tag{3.48}$$

In (3.39), the Laplace-transformed diffusive mass flux, $\tilde{Q}_k$, of radionuclide k at the interface between the bentonite region and the host rock, $r = r_2$, is required. From (3.17–20), (3.24), the analytical solution for the Laplace-transformed concentration, N_k, in the bentonite region, Q_k can be obtained by (3.16) as

$$\tilde{Q}_k = \frac{\varepsilon D_{e(k)} r_1}{r_2}\left\{\frac{\tilde{\psi}_k\phi_k}{Q_{kk}}\exp\left(-\phi_k L\right) + \sum_{i=1}^{k-1}\tilde{\psi}_i\left[\prod_{j=i}^{k-1}(\chi_{m+1}v_m)\right]\sum_{m=i}^{k} a_m^{(j)}\frac{\phi_m \exp\left(-\phi_m L\right)}{\prod_{\substack{j=i \\ j\neq m}}^{k}\left(\phi_j^2 - \phi_m^2\right)}\right\}, \quad k = 1, 2, \ldots, i, \tag{3.49}$$

where $$Q_{kj} = \frac{1}{2}\left\{\left(H_k\phi_j + J_k\right) + \left(H_k\phi_j - J_k\right)\exp\left(-2\phi_j L\right)\right\}, \tag{3.50}$$

$$H_k = \left(1 - \sigma_k\right)\varepsilon D_{e(k)},\ J_k = \sigma_k + \frac{H_k}{r_1},\ \phi_j = \sqrt{\frac{K_{e(k)}}{D_{e(k)}}(s + \lambda_j)}, \chi_k = \frac{D_{e(k-1)}}{D_{e(k)}}, \tag{3.51}$$

$$a_n^{(j)} = \sum_{m=j}^{n-1} a_m^{(j)} \frac{Q_{nm}}{Q_{nn}} \quad \frac{\prod_{l=j,\, l\neq m}^{n-1}\left(\phi_l^2 - \phi_n^2\right)}{\prod_{l=j,\, l\neq m}^{n-1}\left(\phi_l^2 - \phi_m^2\right)}, a_j^{(j)} = \frac{1}{Q_{jj}},\ a_n^{(j)} = 0, n \le j-1, \tag{3.52}$$

$$\nu_k = \frac{K_{e(k)}\lambda_k}{D_{e(k)}}, \nu_0 = 0, \tag{3.53}$$

$$k = 1, 2, \ldots, i$$

See also (3.30) for other definitions. The coefficient $a_n^{(j)}$ is defined in a recursive way. $\bar{\psi}_k$ is the Laplace-transform of $\psi_k(t)$, which is given by (3.25). σ_k in (3.51) is either 1 for the solubility limited boundary condition (3.21) or 0 for the congruent-release boundary condition (3.23), which is determined by calculating the time when the mass of the precipitate, $P_k(t)$, vanishes by (3.34).

3.4 Input Data

Parameter values for the repository configuration, the barrier properties, and the hydrologic conditions in the geologic formation are summarized in **Table 3.1**.

The assumed leach time corresponds to relatively high ambient temperature in the repository [24]. The longitudinal dispersion coefficient is assumed to be zero to obtain conservative results for the maximum concentrations in the host rock. The retardation coefficients for the fracture transport are set to be unity by assuming conservatively that no nuclides are sorbed by the fracture-filling materials. With the assumed fracture spacing of 1 m [5], the number of fractures intersecting the repository is estimated as 2,000.

Table 3.2 summarizes the ranges of solubilities and sorption distribution coefficients in the bentonite and in the rock matrix.

In **Table 1.1**, relevant radionuclides and radioactive decay chains are listed. Among them, fissile radionuclides are ^{245}Cm, ^{239}Pu, ^{235}U, and ^{233}U. From the viewpoint of the criticality scenario, the worst case is the case where accumulation of a high fissile-material enrichment is realized. Considering their relatively long half-lives, the fissile nuclides of primary concern are ^{235}U and ^{233}U. (^{245}Cm and ^{239}Pu are so short-lived that no significant contribution to the accumulation is observed as shown in **Figure 3.5**.) The precursing radionuclides such as ^{245}Cm, ^{241}Am, ^{243}Am, ^{237}Np, ^{242}Pu and ^{239}Pu, will eventually decay to uranium isotopes, and behave as moving sources for the production of uranium.

We make calculations for three representative cases, depending on the magnitudes of the solubilities and sorption distribution coefficients of uranium isotopes and their precursors. **Table 3.2** shows the combinations of parameter values for each of those three cases. In case (a), the upperbound values of the ranges shown in **Table 3.2**(1) are assigned for the solubilities of Cm, Am, Pu, and Np, whereas the lowerbound value is assigned for the solubility of uranium. The lowerbound values of the ranges shown in **Table 3.2**(2) and (3) are assigned for the sorption distribution coefficients of Cm, Am, Pu, and Np in the bentonite and in the host rock,

respectively, whereas the upperbound value is assigned for the uranium sorption distribution coefficients. With such a combination, the total mass of Cm, Am, Pu, and Np existing as solutes in the water phases in the bentonite and in the host rock can be maximized, whereas the mass of uranium in the water phases is minimized. In case (b), the total mass of Cm, Am, Pu, and Np in the water phases is minimized, whereas the mass of uranium in the water phases is maximized. Case (c) is the median case.

Table 3.1 Assumed Parameter Values

Radius of the equivalent spherical waste glass, r_1	0.409 m #
Radius of the equivalent spherical bentonite region, r_2	2.52 m #
Surface area of the waste glass, $S = 4\pi r_1^2$	2.10 m^2
Surface area of the bentonite region, $S_2 = 4\pi r_2^2$	79.8 m^2
Leach time, T_L	4×10^4yr §
Porosity of the bentonite region, ε	0.3 §
Density of the bentonite region, ρ	2100 kg/m^3 §
Porosity of the host rock, ε_p	0.001 ~ 0.5 ‡
Diffusion coefficient in the bentonite, $D_e = \tau D_{e(k)}^v$	3×10^{-2} m^2/yr #$
Density of the host rock, ρ_p	2600 kg/m^3 §
Porosity of the fractures, ε_f	1
Water velocity in fractures, v	1.0 m/yr §
Longitudinal dispersion coefficient, D^L	0
Fracture aperture, $2b$	6.3×10^{-4} m §
Fracture spacing, $2a$	1 m #
Retardation coefficient in the fracture, R_e	1
Intrinsic diffusion coefficient in rock, $D_{e(k)}^i = \varepsilon_p \tau_p D_{e(k)}^v$	10^{-5} m^2/yr *
Repository dimension, L_R	2000 m
Fracture cross-sectional area per glass log, $S_f = 2bL_R n_f / n_w$	0.063 m^2
Number of waste canisters, n_w	40,000 #
Number of fractures intersecting the repository, n	2,000
EBS-NBS interface factor, A	1.58×10^{-3}

§: from Ref. [24] #: from Ref. [5] ‡: from Ref. [25]. 0.01 is used for the present calculation.
$: from Ref. [26]
*: Based on the values for D_e, the rock porosity $\varepsilon_p = 0.01$, and the ratio of tortuosity correction factors, $\tau_p/\tau = 0.055$, given in [24].

To distinguish these three cases, we introduce the factor θ defined as

$$\theta = \frac{\kappa_{U,1}}{\sum_{e=Cm,Am,Pu,Np} \kappa_{e,1}} + \frac{\kappa_{U,2}}{\sum_{e=Cm,Am,Pu,Np} \kappa_{e,2}}, \tag{3.54}$$

where

$$\kappa_{e,1} = \frac{N_e^*}{\sqrt{K_e}} \text{ and } \kappa_{e,2} = \frac{N_e^*}{\sqrt{\alpha_e}}. \tag{3.55}$$

The physical interpretations for $\kappa_{e,1}$ and $\kappa_{e,2}$ can be given as follows. The effective diffusion thickness for element e from the glass log surface in the EBS is proportional to $\sqrt{D_e/K_e}$. The quantity $N_e^*\sqrt{D_e/K_e}$, then, gives the magnitude of the mass of element e existing in the water phase of the EBS. If we assume that the diffusion coefficient D_e is of the same order for the elements we consider here, the mass of element e existing in the water phase of the EBS is proportional to

$\kappa_{e,1}$. Similarly, we can consider the magnitude of the mass existing in the water phase in the host rock matrix surrounding the fractures, which is proportional to $\kappa_{e,2}$. The factor $\theta > 1$ means that more uranium is in the water phases and transportable than the precursors. With the values in **Table 3.2**, the factor θ can be calculated as 1.1×10^{-4} for case (a), 2.4×10^{3} for case (b), and 0.19 for case (c).

Table 3.2 Assumed elemental parameters

(1)*Solubility* N_e^* [mol/m^3]	Range	Case (a) $\theta = 1.1 \times 10^{-4}$	Case (b) $\theta = 2.4 \times 10^{3}$	Case (c) $\theta = 0.19$
Cm	$10^{-4} \sim 10^{-6}$ (1)	10^{-4}	10^{-6}	10^{-5}
Am	$10^{-4} \sim 10^{-6}$ (2)	10^{-4}	10^{-6}	10^{-5}
Pu	$10^{-5} \sim 10^{-7}$ (3)	10^{-5}	10^{-7}	10^{-6}
Np	$10^{-5} \sim 10^{-9}$ (2)	10^{-5}	10^{-9}	10^{-7}
U	10^{-5} (4) $\sim 10^{-7}$ (2)	10^{-7}	10^{-5}	10^{-6}

(2) *In the bentonite*	K_d^e[m^3/kg]	Range of K_e [dimensionless]	Case (a) $\theta = 1.1 \times 10^{-4}$	Case (b) $\theta = 2.4 \times 10^{3}$	Case (c) (9) $\theta = 0.19$
Cm	10 (1)	4.9×10^4	4.9×10^4	4.9×10^4	4.9×10^4
Am	10 (2)(5)	4.9×10^4	4.9×10^4	4.9×10^4	4.9×10^4
Pu	10 (2)(5)	4.9×10^4	4.9×10^4	4.9×10^4	4.9×10^4
Np	0.1 (2)(5) ~ 100 (7)	$4.9 \times 10^2 \sim 4.9 \times 10^5$	4.9×10^2	4.9×10^5	1.5×10^4
U	0.1 (2)(5) ~ 100 (6)	$4.9 \times 10^2 \sim 4.9 \times 10^5$	4.9×10^5	4.9×10^2	1.5×10^4

(3) *In the host rock*	K_{dp}^e [m^3/kg]	Range of α_e (8) [dimensionless]	Case (a) $\theta = 1.1 \times 10^{-4}$	Case (b) $\theta = 2.4 \times 10^{3}$	Case (c) (9) $\theta = 0.19$
Cm	0.01 ~ 25	$26 \sim 6.4 \times 10^4$	26	6.4×10^4	1.3×10^3
Am	0.01 ~ 25 (1)	$26 \sim 6.4 \times 10^4$	26	6.4×10^4	1.3×10^3
Pu	0.025 ~ 25 (2)(5)	$64 \sim 6.4 \times 10^4$	64	6.4×10^4	1.3×10^3
Np	0.001 (2)(5) ~ 100 (7)	$2.6 \sim 2.6 \times 10^5$	2.6	2.6×10^5	8.2×10^2
U	0.0001 (2)(5) ~ 100 (6)	$0.26 \sim 2.6 \times 10^5$	2.6×10^5	0.26	2.6×10^2

(1): Values for Am are substituted. (2): from Ref. [5]. (3): from Ref. [27]. (4): from Ref. [28].
(5): from Ref. [29] (6): from Ref. [30]. (7): Values for U given in [30] are used.
(8): With the rock porosity $\varepsilon_p = 0.01$. (9): obtained by taking square root of (maximum × minimum) of the range.

3.5 Computer Code

A computer code has been developed for the time-dependent mass fluxes of radionuclides at the bentonite surface, (3.49), and accumulation of radionuclides in the host rock, (3.37).

First, the code determines the boundary condition at the waste glass surface, by the precipitation analysis shown in Section 3.2.2. With the analytical solution, (3.34), t_k^* is obtained by solving $P(t_k^*) = 0$ numerically by the bisection method, for which the subroutine DZBREN of IMSL Library [31] has been utilized.

With the determined boundary condition, the Laplace-transformed analytical solutions (3.37) and (3.49) are inverted numerically, based on the Talbot method [32]. The readily available computer program [33] based on this method has been utilized.

3.6 Inner Boundary Conditions

Table 3.3 shows the times t_k^* when precipitate of radionuclide k disappears. By preliminary calculations, we confirmed that with two orders of magnitude difference in the glass leach time (40,000 yr and 4 million yr), t_k^* of the precipitates is insensitive with the glass leach time. All calculations in this report we performed are for the glass leach time of 40,000 yr.

Table 3.3 Input data for radionuclides in a single glass log and time for disappearance of precipitate.

Nuclide	Half-life [yr]	Initial Inventory$ M_k^o [mol]	t_k^* [yr]		
			Case (a) θ=1.1×10^{-4}	Case (b) θ=2.4×10^{3}	Case (c) [9] θ= 0.19
Pu-240	6.57E+03	2.00E-01	3.8 E+04	8.2 E+04	6.0 E+04
U-236	2.34E+07	5.59E-02	9.5 E+07	4.9 E+06	3.2 E+07
Cm-245	9.30E+03	7.55E-03	C	C	C
Am-241	4.58E+02	2.82E-01	C	5.3 E+03	2.9 E+03
Np-237	2.14E+06	4.02	2.4 E+06	2.8 E+07	1.5 E+07
U-233	1.62E+05	1.24E-03	2.4 E+06	7.7 E+05	1.3 E+06
Pu-242	3.76E+05	1.80E-02	2.2 E+05	2.2 E+06	1.0 E+06
U-238	4.46E+09	5.83	5.0 E+08	5.2 E+06	5.0 E+07
U-234	2.45E+05	1.11E-02	2.4 E+06	9.9 E+05	1.8 E+06
Am-243	7.37E+03	4.86E-01	C	5.2 E+04	2.2 E+04
Pu-239	2.44E+04	2.54E-01	8.8 E+04	2.4 E+05	1.6 E+05
U-235	7.04E+08	7.00E-02	5.5 E+08	5.3 E+06	5.6 E+07

$: Same as Table 2.1. Letter 'C' means that no precipitate occurs, and the congruent release boundary condition (3.22) is applied.

3.7 Numerical Results

Figure 3.5 shows the calculation results for the release from the EBS and the accumulation in the host rock. In each of the top (case (a)), middle (case (b)), and bottom (case (c)) rows, there are four figures; the leftmost figure shows the mass fluxes from the bentonite buffer surface as a function of time (discussion is given in Section 3.7.1). The right three figures show the accumulation of radionuclides contributed by one glass log at 10, 100, and 1000 m from the EBS surface (see Section 3.7.2).

3.7.1 Radionuclide Release from EBS

In case (a) (see **Figure 3.5**(a-1), ^{237}Np and plutonium isotopes are released earlier than uranium isotopes from the EBS. ^{233}U is also released earlier than other uranium isotopes because it is the decay daughter of ^{237}Np and accompanies ^{237}Np.

In case (b) (see **Figure 3.5**(b-1)), uranium isotopes are released earlier than the precursors from the EBS surface. The mass fluxes of the precursors are negligibly smaller than those of uranium isotopes. This is because the half-lives of the precursors are much shorter than those of uranium isotopes, except ^{237}Np.

In case (c) (see **Figure 3.5**(c-1)), both uranium and its precursors are observed at the surface of the EBS. In the time period before 200,000 years, the ^{235}U/^{238}U ratio is about 1. Hence, relatively high enrichment accumulation is possible in this time span.

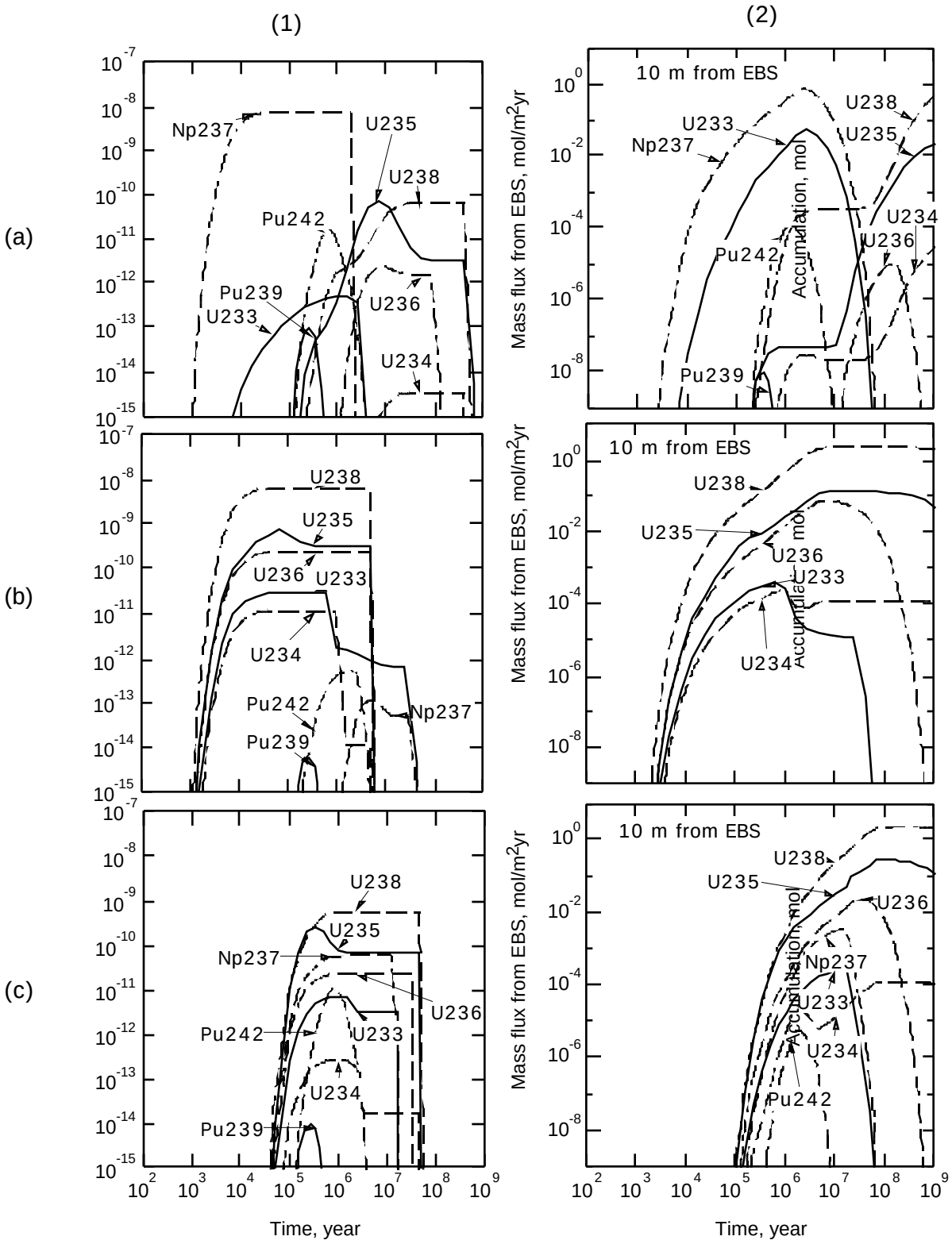

Figure 3.5 Release from the EBS (the leftmost three figures) and the accumulation in the host rock (the three figures in each row), for (a) the precursor-mobile (top row),

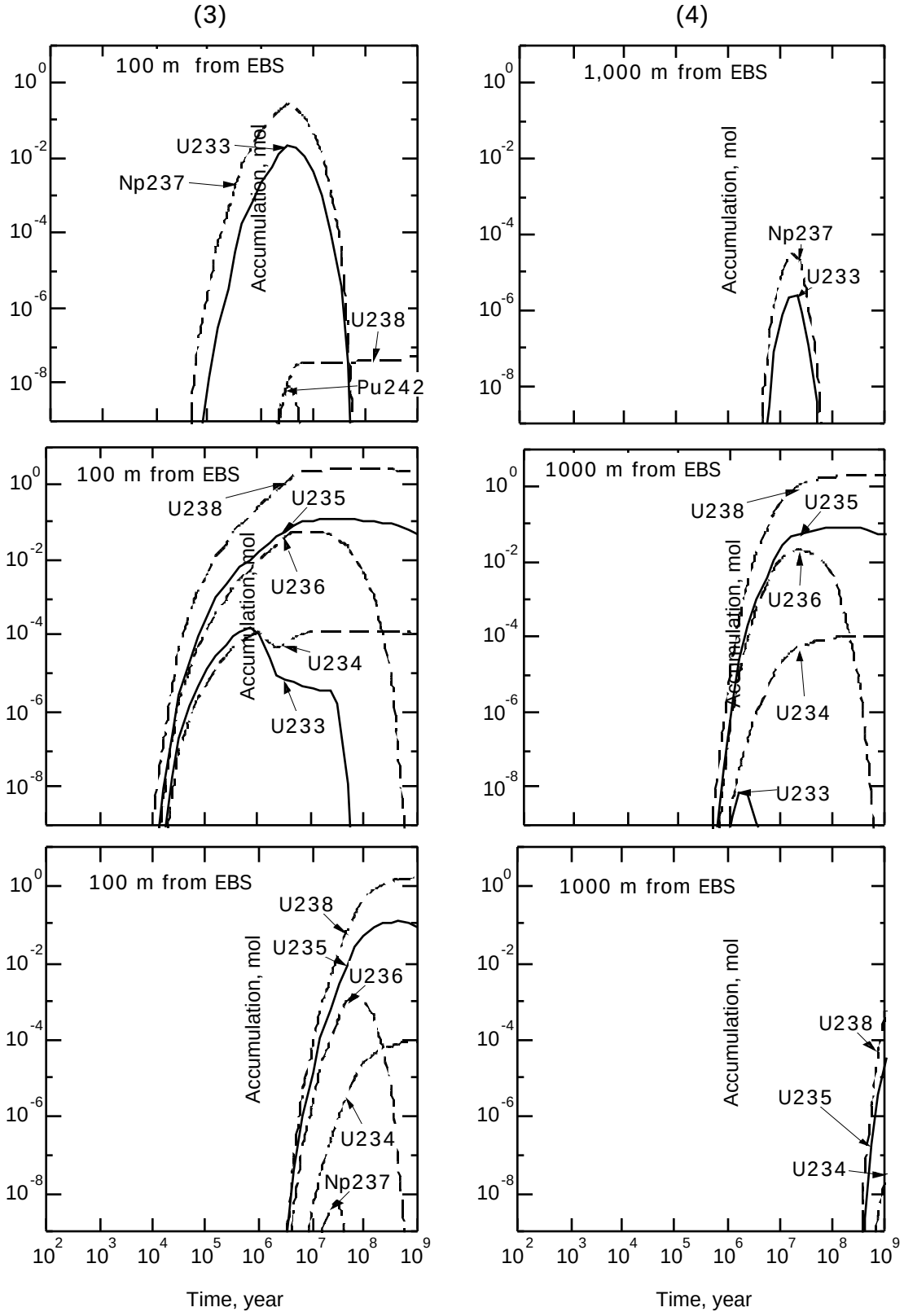

(b) the uranium-mobile (middle), and (c) the median (bottom) cases. The solid and dashed curves represent fissile and poison materials, respectively.

One observes in these three figures that ^{240}Pu, ^{245}Cm, ^{241}Am, and ^{243}Am decay out in the bentonite and will not be released to the fractures, and that the mass flux of ^{239}Pu, one of the major fissile radionuclides, is already very small at the EBS surface. So, we can expect that the amount of ^{239}Pu released from the EBS would be negligibly small in any case.

Thus, important radionuclides for the transport in the host rock are ^{237}Np —> ^{233}U —>, ^{242}Pu —> ^{238}U —> ^{234}U —>, ^{236}U —>, and ^{235}U —>.

3.7.2 Radionuclide Transport and Accumulation in Geologic Formation

The right three figures in each row of **Figure 3.5** show the accumulation of materials at 10, 100, 1000 m locations away from the EBS surface. Here, we assume that all the materials reaching these locations are precipitated out of the water phase and accumulate at the location. The only mechanism that decreases the amount of accumulation is by radioactive decay.

In case (a) (see **Figure 3.5**(a-2), (a-3), and (a-4)), we should concern ourselves about the behaviour of ^{233}U. Because ^{237}Np has a half-life as long as 2.14 million years, it survives the EBS transport, and is transported through the host rock, generating ^{233}U. From **Figure 3.5**(a-2) and (a-3), uranium isotopes other than ^{233}U cannot reach the locations beyond 100 m due to the assumed large retardation coefficient in the rock and low solubility. Because ^{233}U is accompanied by ^{237}Np, a strong neutron absorber (see **Table 1.1**), it would be highly unlikely that the criticality configuration is realized in this case.

Suppose that the accumulation occur 10 m away from the edge of the repository area. From the comparison of **Figure 3.5**(a-4) with (a-3), the contributions from the glass logs located at a distance greater 1000 m from the accumulation point (**Figure 3.6**) will be negligibly small. Within a circle of radius 1000 m, whose center is located at the accumulation point, only 40% of the canisters contribute the accumulation, assuming that all the canisters fail. With a circle of radius 100 m, 0.4%, or 160 failed canisters are included. From **Figure 3.5**(a-2) and (a-3), the maximum ^{233}U accumulation of approximately 0.01 mol from a single glass log occurs at 10^6 yr at 100 m location. Therefore, by 160 failed glass logs within the 100 m radius, only 2 moles of pure ^{233}U will be expected to accumulate. This is too small a mass to create a critical configuration in granite as we observe in Chapter 4.

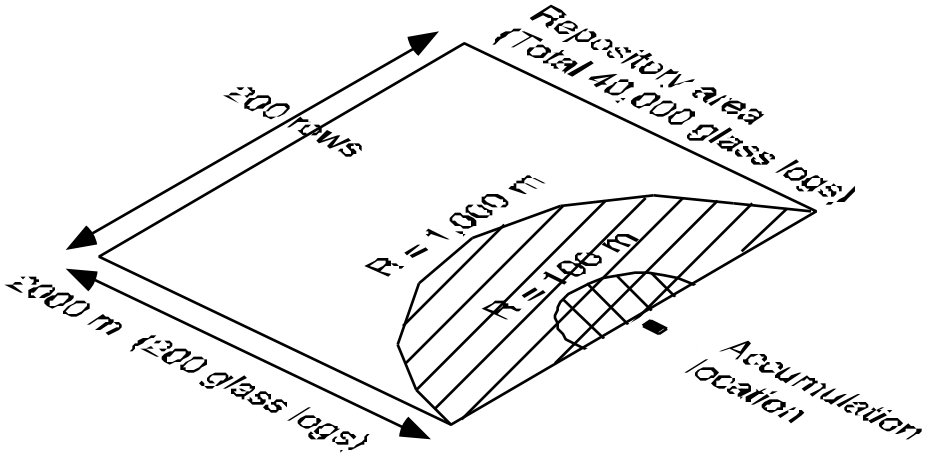

Figure 3.6 Canisters contributing to the accumulation

In case (b), the precursors decay out before they reach the 10 m location, and only uranium is observed there (**Figure 3.5**(b-2)). Due to the long half-lives, assumed greater solubility and smaller sorption distribution coefficients for uranium, approximately one mole of uranium could be precipitated even at the 1000 m location in the host rock, contributed by one

failed glass log. From **Figure 3.5**(b-2), (b-3), and (b-4), the upper bound of the enrichment ($^{235}U/^{238}U + ^{235}U$) is about 12%, but after 10^7 yr, the enrichment reduces to about 8%.

In case (c), we observe that the accumulation starts at 10^5 year at the 10 m location (**Figure 3.5**(c-2)), and 3 million years at the 100 m location (**Figure 3.5**(c-3)). At the 1000 m location, we do not expect significant accumulation of uranium over a billion years (**Figure 3.5**(c-4)). With 160 failed canisters included within the 100 m radius region, only about 200 moles (5 kg) of uranium with 12% enrichment will accumulate. Therefore, in this case, the possibility of the criticality scenario will be negligibly small.

3.8 Concluding Remarks

The important characteristics of vitrified HLW is that it contains the precursors of uranium, Cm, Am, Pu, and Np, whose masses are comparable to that of uranium after reprocessing. They are sources of uranium isotopes. Because their masses are too small for the emplacement criticality event, transport and accumulation must occur to realize a sufficient deposition of TFM, contributed by multiple glass logs to achieve such an event.

From the chemical properties (solubility and sorption distribution coefficients in the bentonite and in the host rock) of the precursor radionuclides (Cm, Am, Pu, and Np) and uranium, we consider the following three cases.

Case (a): Within the assumed ranges, the upper bound values of the solubilities and the lower bound values of the sorption distribution coefficients for the precursors are chosen, so that the masses of the precursors existing in the water phases in the bentonite and in the host rock are maximized, whereas the mass of uranium in the water phases is minimized.

Case (b): The masses of the precursors in the water phases are minimized, whereas the mass of uranium in the water phases is maximized.

Case (c): The median case.

• The mass fluxes of ^{239}Pu (one of the major fissile radionuclides), ^{245}Cm, ^{243}Am, ^{241}Am and ^{240}Pu are already very small at the EBS surface. This has been observed for all three cases considered in this study.

• Thus, important radionuclide for the transport in the host rock are $^{237}Np \rightarrow ^{233}U \rightarrow$, $^{242}Pu \rightarrow ^{238}U \rightarrow ^{234}U \rightarrow$, $^{236}U \rightarrow$, and $^{235}U \rightarrow$.

• In case (a), there is a possibility that highly-enriched ^{233}U deposition is created by decay of ^{237}Np. However, because of assumed strong sorption for uranium, very limited number of canisters can contribute the deposition. Even for the case where all 40,000 glass logs are assumed to contribute the single deposition, the mass of the deposited ^{233}U would be no greater than a kilogram.

• In case (b), uranium can survive more than 1000 m transport in the surrounding host rock. Approximately one mole of uranium could be supplied from one failed glass log to the accumulation point. The ^{235}U enrichment is found to be about 12%. We need further investigation for the mass of the uranium deposition by taking into account the effect of the interference by multiple glass logs (see **Figure 3.1**(b)).

• In case (c), a canister more than 1000 m away from the accumulation location has practically no contribution. Therefore, the number of failed canisters in the repository that can contribute to the deposition would be limited. The mass of accumulated uranium would be no greater than 5 kg with approximately 10 % enrichment.

It should be noted here again that the results obtained above are based on the following assumptions:

• Mass loss due to dispersal during the transport between the release from the glass log to the accumulation is neglected.

• All the radionuclides released from all the glass logs are assumed to migrate toward a single accumulation location.

• Radionuclide release from a glass log is not interfered with radionuclides of the same species released from other glass logs.

Even with these assumptions, cases (a) and (c) above resulted in the TFM accumulation too small for criticality. For case (b), we may need an extended mathematical model and more information about host rocks.

We pass the result of the transport analysis, that is, the possible enrichment of uranium depositions in the host rock would be 12%, and see if the criticality event can occur with this enrichment.

4. CRITICALITY ANALYSIS FOR ACCUMULATED THERMALLY FISSILE MATERIALS

4.1 Introduction

The primary goal of the criticality analysis is to identify the critical configurations which could possibly be formed if large quantities of vitrified HLW were to be placed in the repository.

A fundamental assumption adopted for the criticality analysis is that thermally fissile material (TFM) originating from many canisters will eventually accumulate away from emplacements. The mechanisms which may enable such a reconfiguration of TFM to occur are described and analyzed in Chapter 3 of this report. The thrust of the criticality analysis summarized in this chapter is the search for that combination of TFM and repository constituents which would lead to the minimum critical mass that exhibits positive feedback mechanisms. If this minimum critical mass were found not to be too large to be realizable, it would be necessary to conduct in-depth criticality analysis.

The specific constituents of critical configurations in this part of the work are uranium enriched to 12 atomic percent ^{235}U [U(12)], water, and silica (SiO_2) or granite. The 12% enriched uranium is the neutronically most reactive composition of heavy metal which might be available in large enough quantities to form critical configurations (See Chapter 3). Silica is considered as it is the neutronically least poisonous rock material.

Not just any critical mass is of safety concern. If the reactivity of a critical configuration were to drop as a result of the initiation of a chain reaction (which will cause temperature increase and possibly thermal expansion and water evaporation), the total energy released would be too small to be of any practical significance. Such a system is said to have negative reactivity coefficients or negative reactivity feedback. Critical configurations may have one or more mechanisms of positive reactivity feedback. Section 4.2 identifies various reactivity insertion mechanisms which may play a role in the evolution of an underground chain reaction. Also discussed in Section 4.2 are the conditions under which each of the specific mechanisms may lead to a positive reactivity insertion.

Described in Section 4.3 are the computational methods used for the neutronic analysis, and their benchmarking against selected published critical masses. The computational tools utilized in this study were the same as used in a recent study at UC Berkeley [2–4], where criticality analysis was performed for the case of highly enriched uranium (HEU) and weapons-grade plutonium (w-Pu) disposed of at the proposed Yucca Mountain repository.

Results of our study for $U(12)O_2$-SiO_2-H_2O and $U(12)O_2$-granite-H_2O systems are summarized in Section 4.4. Conclusions from this preliminary study are presented in Section 4.5 along with recommendations for future undertakings.

4.2 Possible Reactivity Feedback Mechanisms

If the effective multiplication factor k_{eff} is greater than unity, the fission power will climb with time as

$$P = P_o e^{\alpha t} \tag{4.1}$$

where the inverse period or "time eigenvalue" α is related to

$$\alpha = \frac{k_{eff} - 1}{\Lambda} \tag{4.2}$$

with Λ being the effective neutron generation time (to be referred to as neutron lifetime). The condition for a large α can thus be translated into a large k_{eff} and a short neutron lifetime. In all supercritical systems, the energy release eventually terminates after negative feedback mechanisms force α to become negative (see **Figure 1.1**).

The reactivity feedback mechanism associated with each of the physical processes that follow the initiation of a chain reaction can be either positive or negative, and has a different amplitude. Thus, to have a large energy release, the following must be met:

- A physical process having a positive reactivity feedback mechanism should be available to initiate the chain reaction.
- The combined reactivity feedback effect of all the physical processes in the system resulting from the chain reaction should be positive, large, and effective, as possible.
- The effects of the physical processes having negative reactivity feedback effects should be delayed as long as possible.
- The neutron lifetime should be as short as possible.

In the following we review the physical processes which may affect the evolution of an underground chain reaction. The primary question addressed in this review is under what conditions, if any, the specific process may have a positive reactivity feedback. Also examined are the conditions which will lead to the shortest neutron lifetime.

4.2.1 Water Removal

Silica, the major constituent of the rock, has a very low thermal neutron absorption cross section. Because oxygen has a relatively low atomic number, SiO_2 is an effective moderator if the "core" size were large enough. In other words, the neutron spectrum in a large enough assembly made of SiO_2 and TFM in which the SiO_2-to-TFM mole ratio is large enough, can be thermal—even without water. The addition of water to such a system can increase the parasitic neutron capture (by neutron absorption in hydrogen, the cross section for which is larger than that of Si), without substantial improvement in the neutron thermalization. The net result of water addition can, thus, be a reactivity loss. If a sufficiently large quantity of TFM has been accumulated in the rock whose void spaces are filled with water, removal of some water would be accompanied by a positive reactivity insertion. In other words, such a system can be over-moderated (see **Figure 1.2** and Section 1.2.2).

To the best of our knowledge, Gore *et al*. [13] were the first to realize that a TFM-SiO_2 system can be critical and well-thermalized. They also realized that the addition of water to such critical systems may have a negative reactivity effect. Bowman and Venneri discussed [1] the possibilities and implications of over-moderation in Pu-SiO_2-H_2O systems as a function of the core size, the Pu concentration (or weight) and the water concentration. A more complete parametric study was recently performed by Sanchez *et al*. in Ref. [17] for Pu fueled systems and in Ref. [34] for HEU fueled systems.

4.2.2 TFM Temperature Increase

If TFM depositions are heterogeneous (rather than homogeneously mixed with the rock), the fission energy released from the chain reaction would first heat deposited TFM. In certain systems, such as the heterogeneous ones considered in this work, the TFM can heat up to very high temperatures before the rock is heated. The primary reactivity effect of the TFM temperature increase is via Doppler broadening[3] of the TFM isotope resonances. It is to be

[3] Since the target nuclei themselves are in thermal motion the relative speed between the neutron and the nuclei may be either greater or less than the neutron speed. Because of this effect, the observed interaction rate of a beam of monoenergetic neutrons depends on the temperature of the target as well as on the neutron energy. As the temperature increases, the resonance broadens, while its peak magnitude decreases.

expected that if the TFM deposition were to contain large enough concentrations of neutron absorbers, such as ^{238}U or ^{240}Pu, Doppler broadening would have a negative reactivity feedback effect with respect to TFM temperature increase.

4.2.3 Rock Temperature Increase

If the chain reaction proceeds, the rock temperature will eventually start increasing. One possible consequence of this temperature increase is acceleration of water removal with its associated positive reactivity feedback. This effect was discussed in Section 4.2.1. Another consequence of the rock temperature increase is neutron spectrum hardening[4].

Consider homogeneous systems (spectrum hardening effects on heterogeneous systems are discussed in Section 4.2.5). In terms of the "four factor formula" for the multiplication factor for a finite system,

$$k_{eff} = f\eta\varepsilon p P_{NL} \tag{4.3}$$

the temperature-induced spectrum variations may affect k_{eff} via, primarily, the thermal utilization, f (the fraction of absorbed neutrons which are absorbed in TFM), η (the average number of neutrons produced per neutron absorbed in TFM) and slightly via the nonleakage probability, P_{NL}. p is the resonance escape probability.

An indication of the first two spectral effects can be obtained from **Figure 4.1** and **Figure 4.2**. Plotted in **Figure 4.1** is the ratio σ_a^U / σ_a^H as a function of neutron energy for different uranium enrichments. This ratio is indicative of the energy dependence of f in homogeneous systems; having a $1/v$ energy dependence, the hydrogen absorption cross section well represents the energy dependence of all the system constituents excluding the uranium isotopes. From **Figure 4.1**, it is expected that, for an initially well-thermalized system, f will continuously decrease with energy increase with several small fluctuations. An exception is the energy range above about 4 eV in which the increase in f is quite significant.

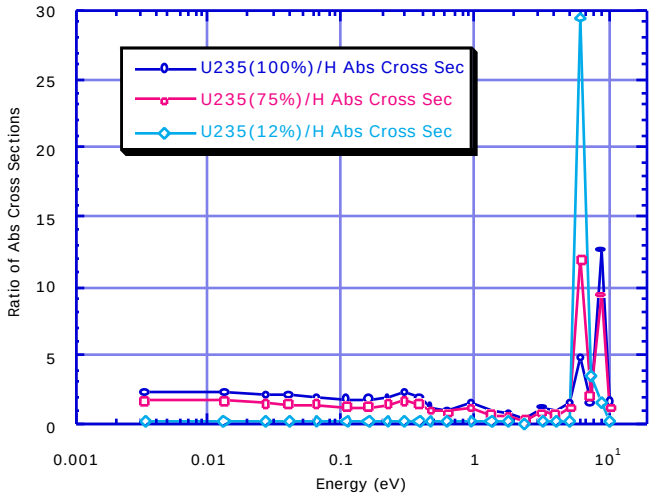

Figure 4.1 Energy dependency of the absorption cross-section ratio.

[4] In a well-thermalized system, an increase in the rock temperature will increase the average neutron energy. This is called spectrum hardening.

Figure 4.2 shows that the η of ^{235}U is almost temperature independent up to about 0.07 eV, and decreases with fluctuation for the neutron energy greater than 0.07 eV. The product $\eta(\sigma_a^{U-235}/\sigma_a^H)$ tends to decline with temperature, when starting from a relatively soft spectrum. Hence homogeneous ^{235}U systems are expected to have a negative reactivity feedback with respect to rock temperature increase while the rock temperature is relatively low. However, it was discovered in [2] that ^{235}U fueled systems, when heterogeneous, can have as large a positive rock-temperature feedback as ^{239}Pu systems.

It should be realized that in most types of nuclear systems, the temperature coefficient of reactivity is negative - both for fuel temperature increase and for moderator temperature increase. This situation is crucial for ease of control and for the safety of nuclear reactors.

Rock temperature increase also causes rock expansion, followed by reduction in material densities. This thermal expansion is expected to have a negative temperature feedback *via* P_{NL}. However, the magnitude of the reactivity effect due to spectrum hardening can be the dominant of the two.

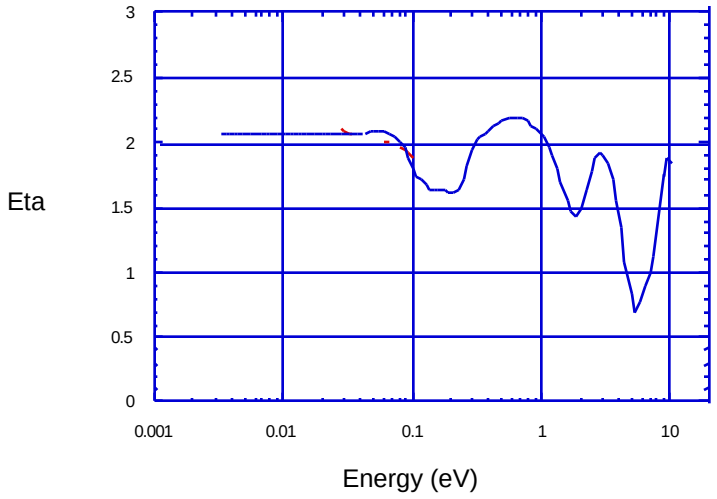

Figure 4.2 Energy dependence of η for ^{235}U.

4.2.4 Dispersion of TFM

It has been pointed out by Bowman and Venneri [1] that the dispersion of a given amount of TFM over a larger volume of rock can result in reactivity increase *via* a reduction in P_{NL}. A number of the critical configurations proposed and analyzed by Bowman and Venneri involve dispersion as the mechanism initiating the autocatalytic criticality event.

Dispersion of a given quantity of TFM over a larger volume affects the neutron balance in two primary ways: (a) reducing the leakage probability (due to increasing the core volume-to-surface ratio), and (b) reducing f. For small enough initial core volumes, the leakage positive reactivity effect is dominant.

However, the situation may be reversed for heterogeneous configurations involving low enriched uranium (LEU). In LEU systems, dispersion of the uranium may lead to reactivity drop due to a reduction in the self-shielding of the ^{238}U resonances. From thermal reactor theory, heterogeneous configurations can be more reactive than homogeneous configurations.

In heterogeneous geometries, like those formed by the deposition of TFM on rock surfaces in fractures, dispersion of TFM may occur as a consequence of the TFM heating up, melting and, later, evaporation.

4.2.5 Heterogeneity and Self-Shielding

Almost all of the criticality safety problems associated with TFM deposited in rock preceding the UC Berkeley study [2–4] assumed a homogenous uniform deposition of TFM. In fact, we are aware of only one study which examined heterogeneous deposition—a study done recently by Parsons *et al.* [35]. The goal of their study was to estimate to what extent segregation of the plutonium into small grains will affect the neutron multiplication of a rock - plutonium system. Their study was done by comparing k_∞ calculated for a pair of cases—one having a homogeneous distribution of the TFM and the other having the same amount of TFM segregated into small grains. They found [35] that for large enough rock-to-TFM mole ratios, the segregation of Pu to small spherical grains, 2.6 or 3.2 mm in diameter, can substantially reduce k_∞ relative to the corresponding homogeneous composition. They attributed the negative reactivity effect of segregation to self-shielding.

The incentive of the study by Parsons *et al.* [35] was to show that the analysis of Bowman and Venneri [1] is over-optimistic; if they were to have taken the self-shielding effects (as well as actual rock composition and actual plutonium composition) into account, some of the critical configurations Bowman and Venneri considered would not be critical at all. Our perception of the effect of segregation is different—segregation provides a mechanism for positive reactivity feedback. Let us analyze, qualitatively, the expected reactivity feedback for HEU and LEU.

In a well-thermalized system fueled with heterogeneous HEU depositions, spectrum hardening caused by rock temperature increase will reduce the effective absorption cross section of the HEU, thus reducing the thickness of the fuel layer as measured in units of mean-free-path for absorption. The net outcome is a reduction in the self-shielding of the fuel and, hence, an increase in f (**Figure 4.3**). It turns out [2–4] that this mechanism is responsible for a positive reactivity feedback due to rock temperature increase in heterogeneous HEU systems. An opposite trend may be found [2–4] in weapons-grade Pu systems when a significant part of the neutrons have energy which is below the 0.3 eV resonance; spectrum hardening in this domain will result in an increase in the effective absorption cross-section and, hence, in an increase in the self-shielding effect. However, in this energy domain the increase in the unshielded plutonium-to-rock absorption cross-section far outweighs the increase in self-shielding.

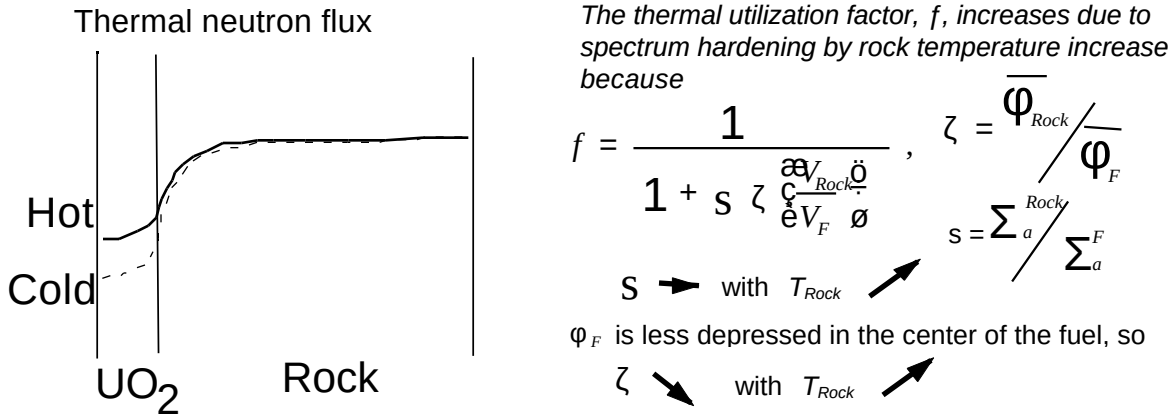

Figure 4.3 Positive feedback mechanism by spectrum hardening and spatial self-shielding.

If the fuel layer were made of LEU, the spectrum hardening effect on reactivity would be expected to be qualitatively similar to the spectrum hardening with HEU—it may reduce the spatial self-shielding effect and thus increase the fraction of neutrons absorbed in the TFM and,

hence, the reactivity of the system. However, spectrum hardening also tends to increase the fraction of neutrons absorbed in ^{238}U relative to the neutron fraction absorbed in ^{235}U. This latter effect will have a negative reactivity feedback. A detailed numerical analysis is required for finding which of the effects will be the dominant for a specific system.

Suppose an heterogeneous system featuring layers of TFM with rock in between becomes super-critical. As a result of fission energy generation, the TFM and, later, the rock material, will start to melt and eventually to evaporate. The change in the state of matter along with the accompanying pressure and temperature gradients created are likely to cause the TFM to mix with the other constituents. The result will be a reduction of the self-shielding with an associated either positive or negative reactivity effect. In systems fueled with HEU, the homogenization is expected to have a positive reactivity feedback (due to an increase in f). However, in systems fueled with LEU, the increase in the resonance absorption in ^{238}U could outweigh the increase in f, making negative the reactivity effect of the homogenization.

Other expected effects of homogenization include reduced leakage (positive feedback) and a small reduction or increase (depending on energy/temperature domain) in η due to spectrum hardening (negative or positive feedback).

4.2.6 Pressure-Driven Expansion

If the chain reaction would evolve to generate large enough fission energy in short enough time, the pressure in the core would eventually build up to such a high level that the core would undergo massive expansion. The increase in the core surface-area - to - volume ratio accompanying such an expansion is expected to increase the neutron leakage probability and, ultimately, to quench the chain reaction. For a given pressure buildup at the center of the core, the larger the core volume, the longer it takes for the expansion to cause a given reactivity drop.

4.2.7 Effective Neutron Lifetime

As discussed in Section 4.2.1, one of the conditions for the configuration with large energy release is a short neutron lifetime. Consider first an infinite system. The average time for a fission neutron to be absorbed can consist of three components: the slowing-down time, t_S, the thermalization time, t_{th}, and the thermal-diffusion time, t_d. Using elementary reactor theory, t_S and t_d can be expressed as follows:

$$t_S = \frac{2}{\bar{\xi}\Sigma_s v_F} \tag{4.4}$$

$$t_d = \frac{1}{\Sigma_{a,T} v_T} \tag{4.5}$$

where

- ξ is the average lethargy increase per collision,
- Σ_s is the average macroscopic scattering cross section in the slowing-down energy range,
- v_F is the speed corresponding to the transition from epithermal to thermal energy range; usually 1 eV,
- v_T is the average speed of the thermal neutrons, and
- $\Sigma_{a,T}$ is the average macroscopic absorption cross section of the thermal neutrons.

Table 4.1 gives, for illustration, values for t_S and t_d, calculated from the above expressions, for several mixtures of SiO_2 (at 2.20 g/cm^3) and water; the values are insensitive to the type of fissile material. In addition to pure SiO_2, we considered a fictitious rock having a thermal absorption cross section twice that of pure SiO_2. The reason for doing this was to obtain an indication on the sensitivity of t_d to different rock compositions (t_S is not sensitive to such a

difference). It is observed that (1) the thermal diffusion time is the dominant contribution to the neutron lifetime; (2) the water concentration has a very significant effect on the thermal diffusion time and, even more so, on the slowing-down time; and (3) the higher the absorption probability of the non-SiO_2 constituents of the rock, the shorter is the diffusion time. The shortest neutron lifetime to be expected in underground thermal critical systems is of the order of few tenths of a millisecond.

Table 4.1 Effects of Water Concentration and Fractional Increase in Rock Absorption Cross-Section on Slowing-Down and Thermalization Times for Infinite Homogeneous Media [2]

Water Density (g/cm^3)	t_S (μs)	t_d (μs) for $\Sigma_{a,T}$ (SiO_2)	t_d (μs) for $2\Sigma_{a,T}$ (SiO_2)
0.05	15.6	673	336
0.1	9.1	413	256
0.2	4.9	298	207
0.4	2.6	192	149

4.3 Computation Method

4.3.1 Monte Carlo Code MCNP

The MCNP (Monte Carlo Neutron-Photon) code [36], developed in the Radiation Transport Group (X-6) of the Applied Theoretical Physics Division (XTM Division) at the Los Alamos National Laboratory has been used for all the neutronic calculations reported upon hereafter. The MCNP cross section library which we had was derived mainly from the ENDF/B-IV evaluation, as available in the DLC-105 RSIC data library.

The free gas model of MCNP has been used to account for the upscattering of thermal neutrons, by all constituents other than water. The S(α, β) treatment is used to describe scattering by water molecules for media temperatures up to 800 K. Above this temperature, the free-gas model is used for scattering from water as well (there is no S(α, β) data for water above 800 K). MCNP does not have a built-in algorithm to account for the effect of temperature increase on Doppler broadening of resonances. We had access to the cross section libraries generated for a limited number of above-room temperatures.

4.3.2 Benchmarking

The Monte Carlo MCNP code and its associated cross section libraries have been benchmarked against measured and calculated critical data reported upon in [37]. Two families of uranium-water systems have been considered: one using 5% enriched uranium and the other using 30.3% enriched uranium. These were the enrichment levels reported upon in [37] which bracket the U(12) of interest to the present work. The benchmark systems are moderated and reflected by water.

Figure 4.4 shows the results of the benchmarking. The figure represents results given in [37], upon which we have superimposed our own calculated results. Our calculated results are in very good agreement with those published in [9] for both enrichment levels. The statistical accuracy of all the calculated multiplication factors has been found to be better than 0.5%.

Referring to **Figure 4.4**, it is seen that the minimum critical mass of U(12) in water is between 1 and 2 kg of ^{235}U. The corresponding minimum critical volume of a spherical core is obtained between 20 and 40 liters, that is, between 16.8 and 21.2 cm in radius.

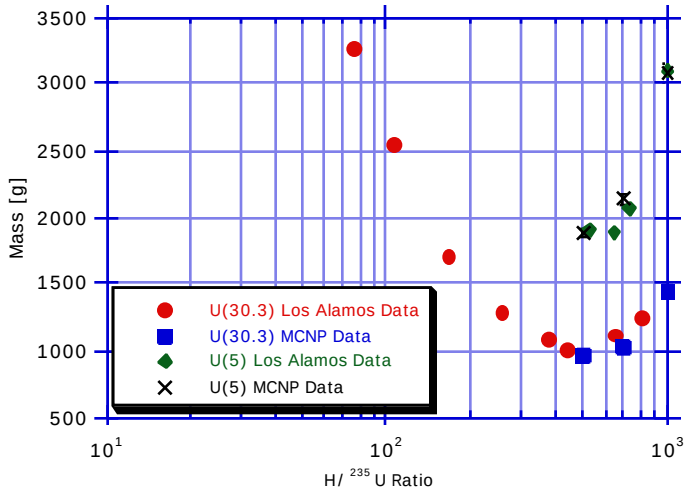

Figure 4.4 Critical masses of ^{235}U in water-reflected cores of UO_2F_2 solution.

4.4 Criticality Phenomena with the System of U(12)O_2, Rock, and Water

4.4.1 Introduction

If the minimum mass of 12% enriched uranium needed for attaining an underground critical configuration were too large to be of practical interest, there would be no need to embark upon a thorough study of critical configurations made of U(12). Hence, the first undertaking in the neutronic evaluation of the criticality of 12% enriched uranium is to establish the minimum mass of this material required to make a critical configuration in either water-saturated silica or granite (Section 4.4.2). The systems considered for this study are reflected spherical cores of uniform homogeneous composition.

The next question addressed is what is the minimum critical mass that is over-moderated. Suppose that a chain reaction would somehow be initiated in a critical system. As a result of the fission energy release, the system temperature would start to increase. This temperature increase would cause the water first to expand (the volumetric coefficient of expansion of water is significantly larger than that of rock) and later, possibly to evaporate. If the critical system were under-moderated, the expulsion of water would lead to a decline in its reactivity and, hence, to the quenching of the chain reaction. The total expected energy release from such a system is likely to be of no harmful consequences. On the other hand, if the system were initially over-moderated, the expulsion of water would have a positive reactivity feedback which may trigger other positive feedback mechanisms, if any, leading to significant fission energy release. The transition from undermoderation to overmoderation conditions is a function of the core size and composition. Generally speaking, the reactivity effect due to water removal becomes less negative or more positive the larger is the core volume and the water contents. Section 4.4.3 summarizes our findings about this transition point for several water concentrations. It is found that the critical mass corresponding to this transition point is not too large to justify putting the underground criticality concern to rest.

Section 4.4.4 examines two other important reactivity feedback mechanisms: Doppler broadening of resonances, and neutron spectrum hardening. In homogeneous systems these two

effects act simultaneously. However, in heterogeneous systems, Doppler broadening comes earlier, as there is some time delay between the fission energy release in the uranium layer, and the heat transfer to the adjacent rock.

It is shown in [2] that the Doppler effect in uranium systems having more than about 90% ^{238}U is negative, and that spectrum hardening in HEU systems has a negative feedback when the HEU deposition in rock is homogeneous whereas it has a significant positive feedback when the HEU deposition is heterogeneous. Based on these findings, we expect spectrum hardening in homogeneous U(12) systems to have negative feedback as well. The question addressed in this section is, therefore, whether or not heterogeneous critical systems of U(12) can have positive reactivity feedback due to spectrum hardening. Another important question touched upon is whether or not there can be a heterogeneous U(12) critical system in which the combined reactivity effect of Doppler broadening and spectrum hardening is positive.

In Section 4.4.5, examined is homogenization as the fourth reactivity feedback effect. As is well known from thermal reactor physics, heterogeneous configurations of natural or LEU fuel have a higher reactivity than homogeneous configurations. The question examined is whether homogenization of heterogeneous critical configurations of U(12) could have a positive reactivity feedback. Homogenization was found to offer a significant positive feedback in case of heterogeneous HEU systems [2].

4.4.2 Minimum Critical Mass

Figure 4.6 and **Figure 4.7** summarize the results from a parametric study of uniform homogeneous spherical cores of $U(12)O_2$ in SiO_2 with 10% fully saturated porosity which are reflected by a 120 cm thick shell of SiO_2 with 0.1 gm/cm^3 water (**Figure 4.5**). The parametric variables of this study are the core radius and the $U(12)O_2$ concentration required for criticality. The SiO_2 is taken to represent the most conservative rock material (leading to the lowest critical mass). Its density is assumed to be 2.20 g/cm^3 . The non-monotonous behavior of the plots of **Figure 4.6** is a reflection of the stochastic nature of the Monte Carlo method. It is found (See **Figure 4.6**) that the minimum critical mass is 17 kg of ^{235}U, which corresponds to 142 kg of U(12). The core radius for the minimum critical mass is 71 cm.

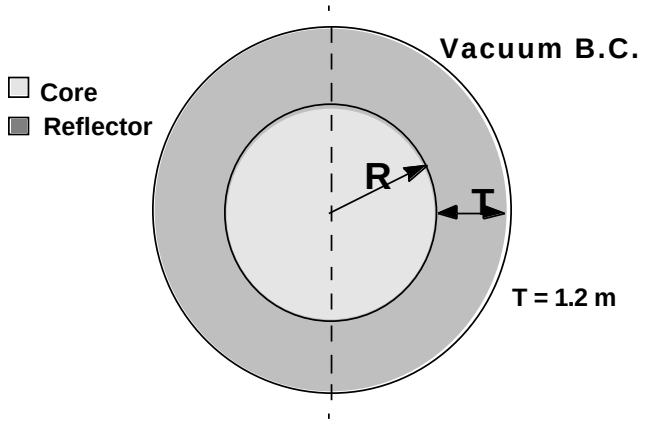

Figure 4.5 Spherical core geometry

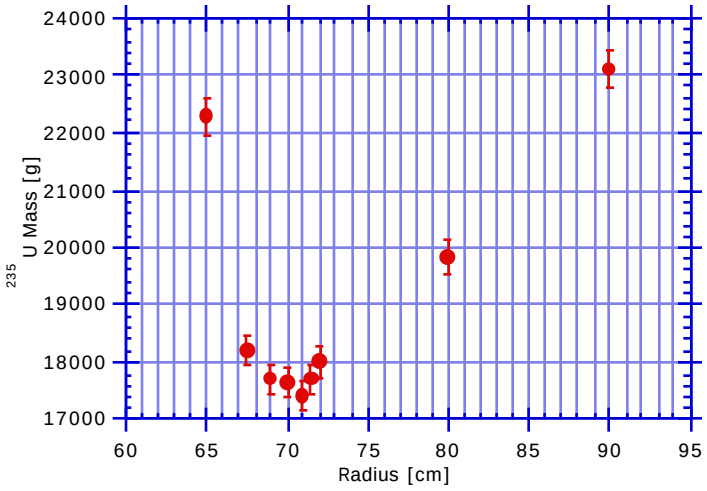

Figure 4.6 Critical masses of ^{235}U in reflected homogeneous spherical cores of $U(12)O_2$ in saturated SiO_2 having 10% porosity.

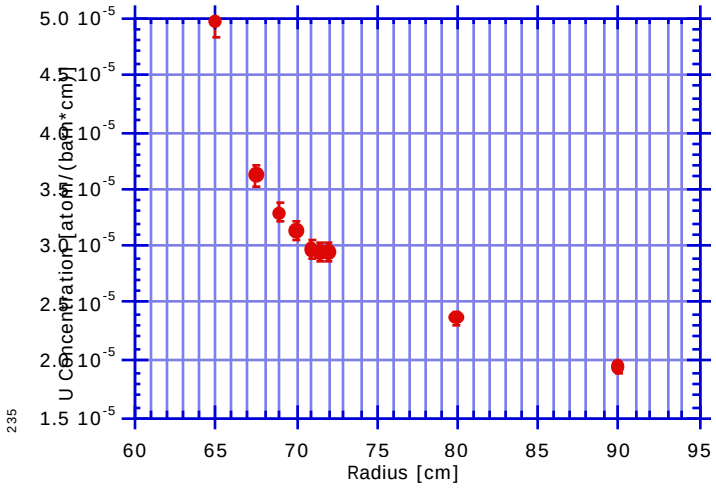

Figure 4.7 Critical concentrations of ^{235}U in reflected homogeneous spherical cores of $U(12)O_2$ in saturated SiO_2 having 10% porosity

Figure 4.8 and **Figure 4.9** summarize the results of a similar parametric study which used granite rather than SiO_2 for the rock. The composition assumed for the granite is summarized in **Table 2.2**; it is obtained by averaging the composition of granite samples taken from several sites in Japan. The porosity of the granite is assumed to be 10%. The minimum critical mass is found to be 60 kg of ^{235}U, which corresponds to 480 kg of U(12). The minimum critical mass core radius is 90 cm. The ^{235}U concentration required for the minimum critical mass configuration is nearly 5×10^{-5} atom/(b•cm) versus about 3×10^{-5} atom/(b•cm) for the SiO_2 system (See **Figure 4.7**). The ^{235}U concentration in the granite need to be higher because the neutron absorption cross section of granite is higher than that of SiO_2.

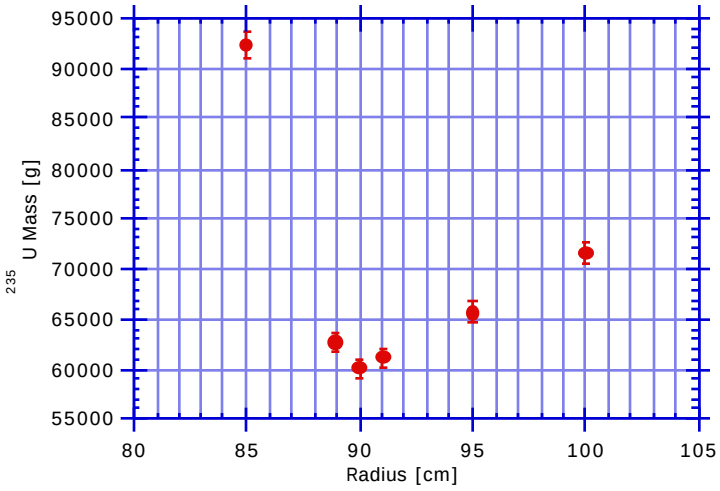

Figure 4.8 Critical masses of ^{235}U in reflected homogeneous spherical cores of $U(12)O_2$ in saturated granite having 10% porosity

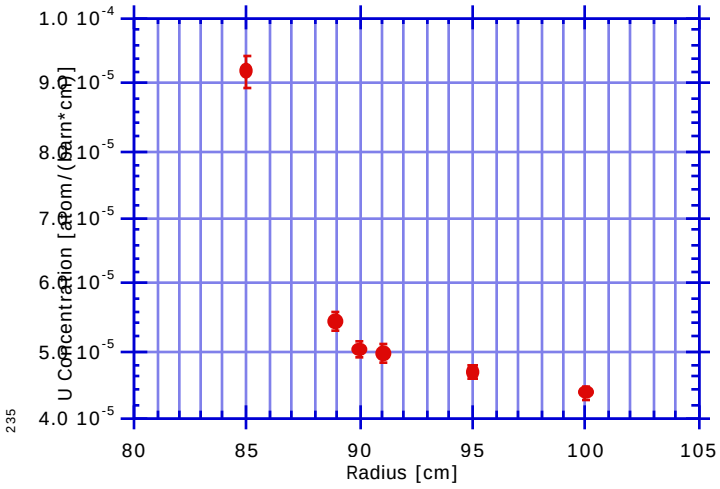

Figure 4.9 Critical concentrations of ^{235}U in reflected homogeneous spherical cores of $U(12)O_2$ in saturated granite having 10% porosity

The probability of accumulation of nearly half a ton of U(12) in a volume of less than 4 m^3 is likely to be very small. Hence, we examined the effect of an increase in the water-to-granite volume ratio on the minimum critical mass. **Figure 4.10** and **Figure 4.11** summarize our findings for a medium consisting of 70 volume % granite and 30 volume % water; such a medium may exist in highly fractured zones. It is found that the water content has a very strong effect on the minimum critical mass and on the corresponding core volume. (This is consistent with the information provided in **Figure 4.4**.) The minimum critical mass is 7 kg of ^{235}U, which corresponds to approximately 57 kg of U(12). The minimum critical mass core radius is 37 cm.

The ^{235}U concentration required for the minimum critical mass configuration is about 8.4×10^{-5} atom/(b•cm).

It is concluded that the minimum critical mass of U(12) in granite rock can be small enough to deserve careful attention. The next question, then, is what mass of U(12) need be deposited in a given rock volume to form a critical mass which exhibits positive reactivity feedback mechanisms.

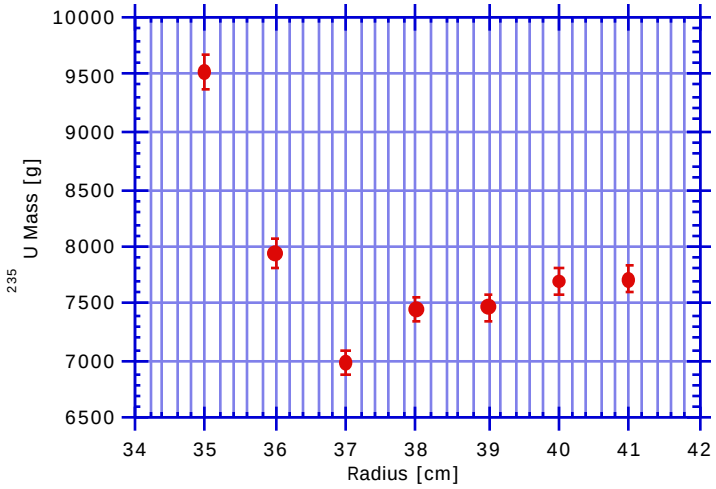

Figure 4.10 Critical mass of ^{235}U in reflected homogeneous spherical cores of $U(12)O_2$ in saturated granite having 30% porosity

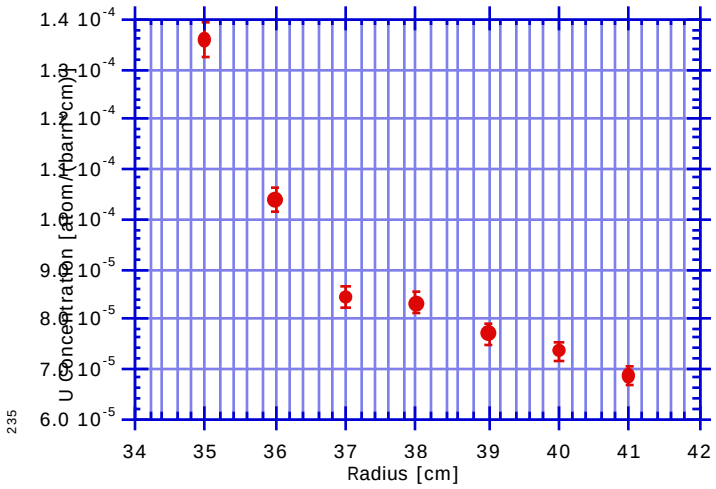

Figure 4.11 Critical concentrations of ^{235}U in reflected homogeneous spherical cores of $U(12)O_2$ in saturated granite having 30% porosity

4.4.3 Reactivity Effect of Water Removal

Figure 4.12 shows the effect of 10% decrease in the water concentration (core and reflector) on k_{eff} of initially critical spherical systems of $U(12)O_2$ + SiO_2(10% porosity) + water. It is found that the transition between under-moderated and over-moderated systems occurs at a core radius in the vicinity of 130 cm. The critical mass for a spherical core 130 cm in radius is 400 kg U(12). This is about three times larger than the absolutely minimal critical mass.

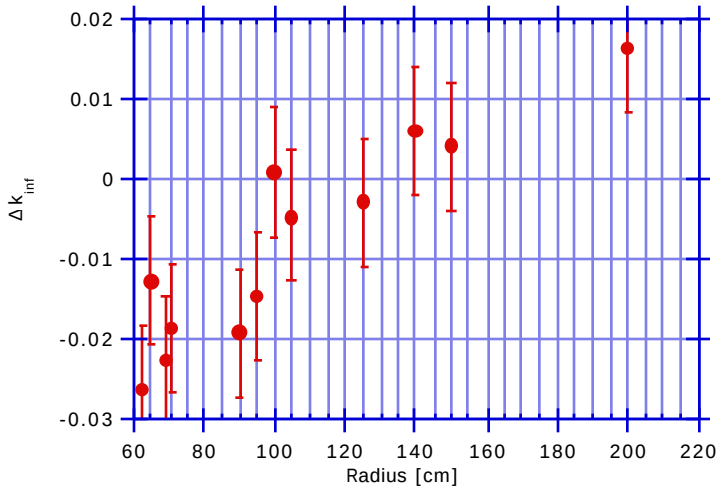

Figure 4.12 Reactivity feedback due to 10% dehydration in core and reflector $U(12)O_2$-SiO_2-H_2O systems defined in **Figure 4.6** and **Figure 4.7**.

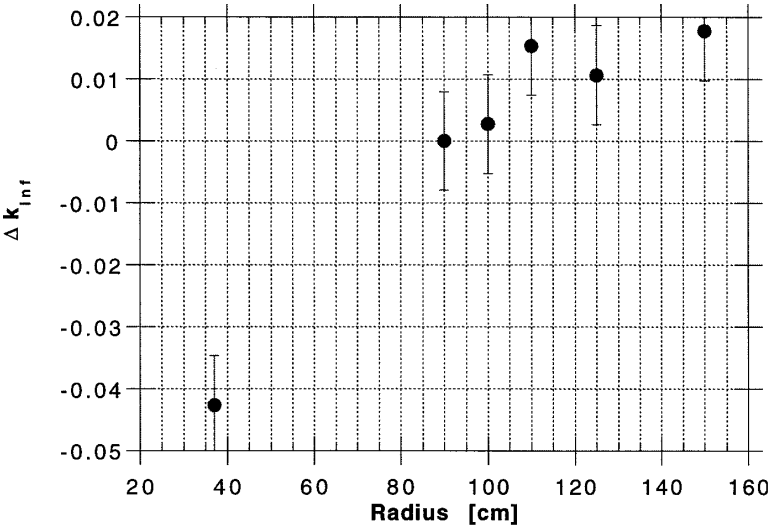

Figure 4.13 Reactivity feedback due to 30% dehydration in core and reflector $U(12)O_2$-Granite-H_2O systems defined in **Figure 4.10** and **Figure 4.11**.

A search for the transition from under- to over-moderation in saturated *granite* having 10% porosity revealed that such systems can not be over-moderated. This is because the fraction of neutrons absorbed by water in such granite-based systems is significantly smaller than in SiO_2-based systems. However, the higher the initial water contents, the larger is the likelihood that the granite systems will be over-moderated. We therefore have sought the under-

moderated/over-moderated transition point in a granite system with 30% porosity. **Figure 4.13** shows the effect on reactivity of a 10% dehydration in the core and reflector. The moderation transition point occurs at a radius of approximately 90 cm with a critical ^{235}U mass of 35 kg.

4.4.4 Reactivity Effect of Temperature Increase

As shown for HEU in [2], Doppler broadening has a negative reactivity feedback when the ^{238}U concentration exceeds about 10 %. A crucial question is whether spectrum hardening due to rock temperature increase can have positive feedback for U(12) fueled systems. If it could, another crucial question would be whether the positive reactivity feedback due to spectrum hardening could be larger than the negative reactivity feedback due to Doppler broadening. Based on the discussion in Section 4.2.3 and Ref. [2], we expect that in homogeneous systems of U(12), spectrum hardening would have a negative reactivity feedback. We shall, therefore, focus on heterogeneous systems of U(12); heterogeneous HEU systems exhibited positive spectrum hardening reactivity effect, as illustrated in [2].

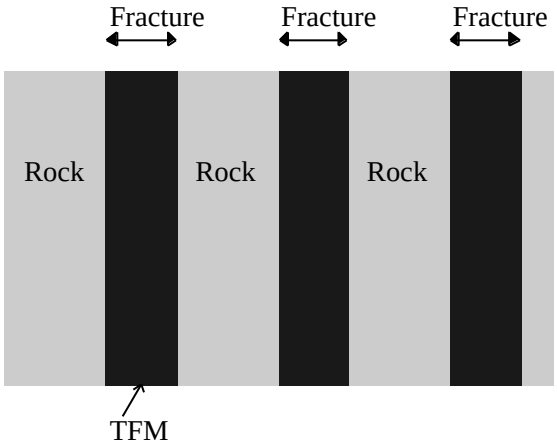

Figure 4.14 Schematic representation of the infinite lattice systems studied.

The infinite heterogeneous lattice (see **Figure 4.14**) consists of a one-dimensional slab unit cell made of a layer of $U(12)O_2$ and a layer of SiO_2 . The latter has a porosity of 10% and is fully saturated. Three thicknesses of $U(12)O_2$ layers are considered: 0.2 mm, 1.0 mm, and 10.0 mm. To each of these TFM (uranium) thicknesses a SiO_2 layer thickness which makes the infinite lattice critical is obtained, as tabulated in **Table 4.2**.

It is found in **Figure 4.15** that if the $U(12)O_2$ deposition layer were thick enough, increase in the rock temperature would have a positive reactivity effect. The more diluted the uranium will be, the lower the spectrum hardening effect is expected to be. The strong dependence of the spectrum hardening effect on the uranium layer thickness is due to the spatial self-shielding dependence on the uranium and rock layer thicknesses; the more heterogeneous the lattice is, the larger will be the self-shielding effect and the more pronounced will be the spectrum hardening effect.

This study has been repeated for infinite slab geometries with granite rock layers having 30% porosity. Three TFM layer thicknesses were considered as before (0.2 mm, 1 mm, and 10 mm). The required critical rock layer thicknesses appear on **Figure 4.16** along with the k_∞ temperature dependence. The k_∞ behavior with rock layer temperature increase for the granite at 30% porosity is nearly identical to that of the SiO_2 at 10%.

Table 4.2 Critical SiO_2 Layer Thickness (cm) of Infinite Lattices Made of $U(12)O_2$ of Selected Thicknesses

SiO_2/H_2O Density [g/cm^3]	SiO_2 Layer Thickness [cm]		
	$U(12)O_2$ Layer Thickness [mm]		
	0.2	1.0	10
2.20/0.1	5.24	13.80	22.60
1.96/0.2	4.00	10.08	16.18
1.71/0.3	3.24	7.90	12.60

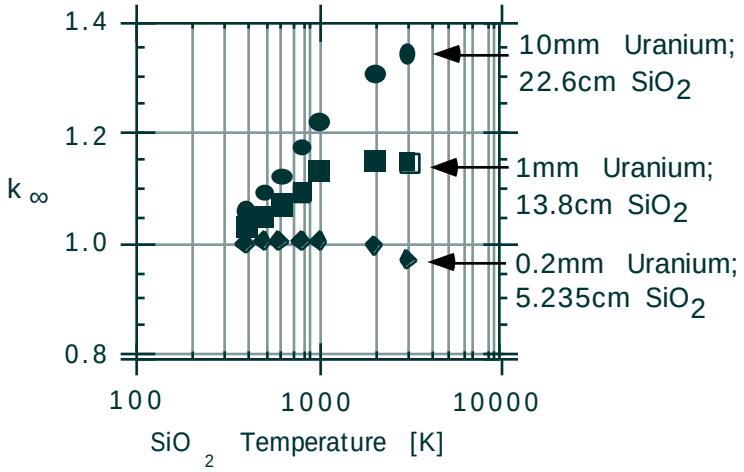

Figure 4.15 Effect of rock temperature increase on k∞ of heterogeneous lattices of U(12)O2 and SiO_2 having 10% porosity.

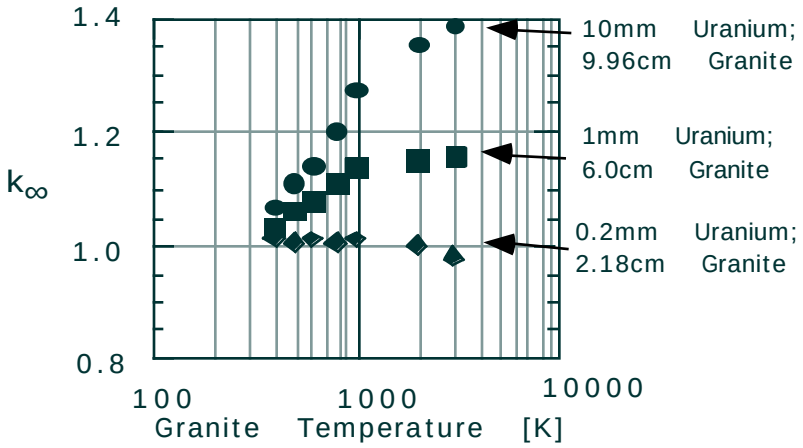

Figure 4.16 Effect of rock temperature increase on k_∞ of heterogeneous lattices of $U(12)O_2$ and granite having 30% porosity.

Let us turn now to the combined effect of Doppler broadening of uranium resonances and spectrum hardening. **Table 4.3** shows the change in k_∞ of the initially critical heterogeneous lattice having 1mm thick $U(12)O_2$ layer as a result of changing the fuel temperature and the rock temperature. It is observed that whereas changing only the fuel temperature has, as expected, a negative reactivity effect, the combined effect of rock and fuel temperature change has a positive reactivity effect (see the diagonal cells of **Table 4.3**). That is, the spectrum hardening reactivity feedback is stronger than the Doppler reactivity feedback.

Table 4.3 Effect of Fuel and Rock Temperature on k_∞ of a Lattice of 1mm U(12)O_2 and 13.8cm SiO_2.

Fuel Temp. [K]	k_∞		
	Rock Temp [K]		
	293	587	881
293	**1.000**	—	—
587	0.997	**1.068**	—
881	0.989	—	**1.090**

4.4.5 Reactivity Effect of Homogenization

Table 4.4 illustrates the effect, on k_∞, of mixing the U(12) and rock layers of selected heterogeneous lattices into uniform homogeneous mixture (i.e., a complete homogenization). It is observed that homogenization has a large reactivity feedback potential. The thicker the uranium deposition layer and the larger the water contents, the larger is the homogenization effect on reactivity.

Table 4.4 Effect of Homogenization on the Infinite Multiplication Constant of the Infinite Lattices Defined in **Table 4.2**.

SiO_2/H_2O Density [g/cm^3]	k_∞		
	U(12)O_2 Layer Thickness [mm]		
	0.2	1.0	10
2.20/0.1	1.0535	1.2654	1.3872
1.96/0.2	1.0706	1.3193	1.4911
1.71/0.3	1.0841	1.3470	1.5264

4.5 Discussions

4.5.1 Spatial Self-Shielding Temperature Dependence

Consider, first, an infinite homogeneous medium made of rock and 0.1 g/cm^3 water. Let us add to this system either U(12), ^{235}U or ^{239}Pu so as to make k_∞ unity, when at room temperature. Let us now increase the medium temperature and check the spectrum hardening effect on k_∞. We shall simulate the spectrum hardening effect by approximating the neutron spectrum to be a Maxwellian, and approximating k_∞ by $\eta f = \nu \Sigma_f / \Sigma_a$. **Figure 4.17** shows the obtained trends of spectrum hardening effect. These are consistent with the results of detailed solutions of the transport equation for HEU and ^{239}Pu systems reported in Ref. [2-4]. The positive spectrum hardening reactivity effect in the ^{239}Pu system is due to the pronounced 0.3 eV resonance of ^{239}Pu [2-4]. The strong decline in the spectrum hardening effect on the U(12) system above 10^4 K is due to the effect of the low lying resonance of ^{238}U. Notice, though, that the effect of the ^{238}U is negligible below 6000 K. Hence, we can conclude that the spectrum hardening reactivity effect in thermal homogeneous critical configurations made of U(12) is very similar to that of the corresponding HEU systems up to above rock melting temperatures.

Consider, next, infinite critical lattices made of heterogeneous unit cells like those referred to in **Figure 4.15** and **Figure 4.16**. Spectrum hardening affects k_∞ primarily via its effect on the "thermal utilization", f,

$$f = \frac{1}{1 + \frac{V_M}{V_F}\,\frac{\bar{\Sigma}_{aM}\bar{\varphi}_M}{\bar{\Sigma}_{aF}\bar{\varphi}_F}}, \tag{4.6}$$

in which $\bar{\Sigma}_{aX}\bar{\varphi}_X$ is the average absorption rate in the rock ($x = {}_M$) and fuel layer ($x = {}_F$). Spectrum hardening affects the absorption rate ratio in two inter related ways: (a) Changing the spectrum average absorption cross section, and (b) Changing the flux spatial distribution, to be measured by the "disadvantage factor" $\zeta \equiv \varphi_M/\varphi_F$. In case of Pu, Σ_{aF} initially increases due to the pronounced 0.3 eV resonance. As a consequence, the spatial self shielding, and hence ζ, also increases. The net result is that spectrum hardening in heterogeneous Pu systems does not have as positive reactivity effect as in homogeneous Pu systems. In case of U, Σ_{aF} decreases with spectrum hardening, and so does ζ. The decrease in ζ causes f, and hence, k_∞ to increase. These trends are illustrated in **Figure 4.18** and **Figure 4.19**; they pertain to unit cells made of 1mm thick fuel layer and rock with 0.1 g/cm^3 water. The rock layer thickness is adjusted to make the room temperature $k_\infty = 1.0$.

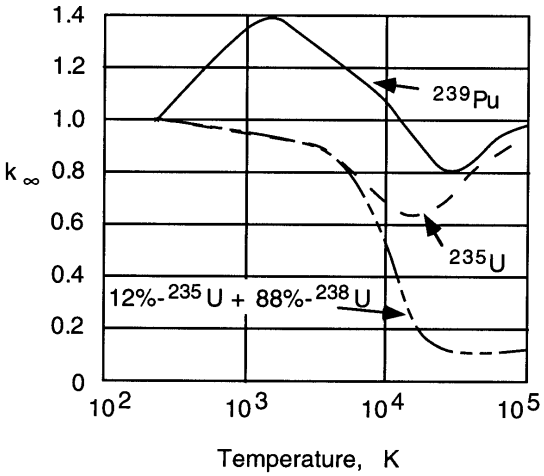

Figure 4.17 Effect, on k_∞, of change in neutron temperature in infinite homogeneous rock with 10% fully saturated porosity made critical by either U(12), HEU or ^{239}Pu.

As a measure of the self-shielding we show in **Figure 4.18** the ratio of the neutron absorption rate in the outermost 1/5 of the fuel layer to the neutron absorption rate in the inner-most 1/5 of the fuel layer, as calculated with MCNP. The results are normalized to the value at room temperature. It is observed that spectrum hardening indeed increases the self-shielding (i.e., flux depression) in the Pu layer, but decreases it in the U layer. **Figure 4.18** shows the overall effect of spectrum hardening on the spatial self-shielding factor while **Figure 4.19** gives the corresponding effect on k_∞ of the two unit cells. The Pu unit cell k_∞ increases with rock temperature despite of the negative contribution of the self-shielding because the spectrum hardening decreases Σ_{aM}/Σ_{aF} more than it decreases ζ.

4.5.2 Critical Mass in Heterogeneous Systems

With HEU or plutonium as the fissile material, the critical mass in heterogeneous systems was found to be larger than in the corresponding homogeneous systems [2, 3]. The scope of the present work was too limited to enable us to calculate the minimum critical mass of heterogeneous systems of U(12). Nevertheless, we can estimate the effect of heterogeneity on the minimum critical mass (MCM) by comparing the average critical concentration we calculated for infinite heterogeneous and homogeneous systems.

Consider the SiO_2 with 10% porosity medium. The critical ^{235}U concentration when $U(12)O_2$ is homogeneously and uniformly mixed in the infinite medium is calculated, with MCNP, to be 3.87 mg/cm^3. If we were to completely homogenize the critical heterogeneous lattice having 0.4 mm thick $U(12)O_2$ layers and 10.47 cm thick rock, the average ^{235}U concentration will be 4.37 mg/cm^3, i.e., only 12.7% higher than in the corresponding homogeneous media. The average critical concentration in the heterogeneous lattices having 2 mm thick $U(12)O_2$ layers is larger than that with 0.4 mm layers by 89% (the ratio of urania-to-rock layer thicknesses). Hence it is concluded that MCM of heterogeneous depositions of $U(12)O_2$ that have positive spectrum hardening reactivity coefficient is less than twice the MCM for homogeneous systems reported upon in this work.

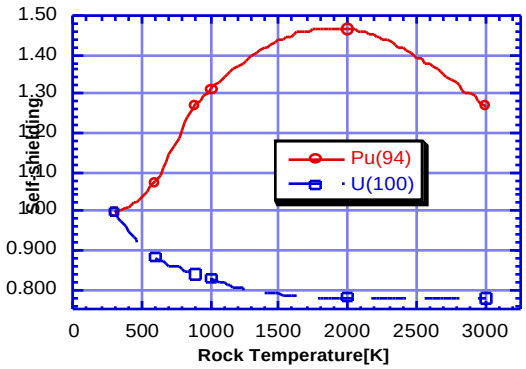

Figure 4.18 Spectrum hardening effect on the absorption rate depression in 1 mm thick fuel layers in heterogeneous unit cells.

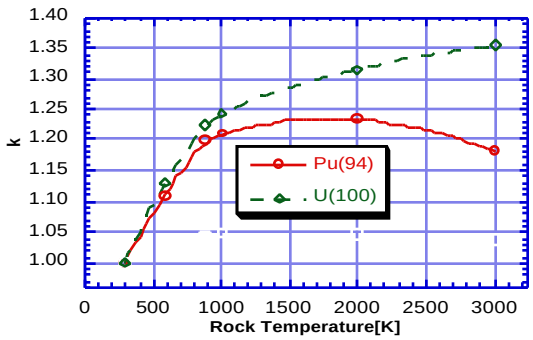

Figure 4.19 Spectrum hardening effect on k_∞ in heterogeneous unit cells with 1 mm thick layer of 94% $^{239}PuO_2$ or $^{235}UO_2$.

4.5.3 On Segregation of the U(12) Deposition

It is very unlikely that the U(12) which may be carried away from the emplacements will be deposited in 0.2 mm or thicker layers of pure $U(12)O_2$. Let us assume that the U(12) will be deposited in concentration equivalent to the highest concentration found in uranium ores. The highest concentration we are aware of is that found in Pena Blanca [2, 3]; it is approximately 10 weight %. At this concentration it will take a layer of approximately 0.7 cm to provide the same amount of U(12) as contained in 0.2 mm of $U(12)O_2$ at 10.96 g/cm^3. At this Pena Blanca like

concentration the uranium deposition can still be heterogeneous; its spectrum hardening reactivity effect might be positive, although not as positive as for the undiluted U(12)O_2 layer of same U contents per layer surface area.

4.5.4 On the Critical Core Volume

Even though the theoretical maximum quantity of U(12) for accumulation might be as large as 10,000 kg (See Chapter 3), it appears that it is very unlikely that at least 290 kg of U(12) will be deposited in a volume which is only about 3 m^3 (corresponding to 35 kg ^{235}U in a sphere 90 cm in radius; see **Table 4.5**). It will be useful, though, to quantify such a probability.

4.5.5 Means for Reducing Criticality Probability

If the above probability will turn out to be large enough to be of concern for the repository design, it will be possible to apply engineering measures that will reduce it. A simple engineering measure would be to add some depleted uranium to the HLW, thus reducing the maximum uranium enrichment level.

4.6 Summary, Conclusions and Recommendations

Table 4.5 summarizes the minimum critical masses of uranium enriched to 12% ^{235}U [U(12)] in different media found in this work. Also given in **Table 4.5** are the radii of the corresponding spherical cores. Each of the cores is surrounded by, essentially, an infinite reflector having the same composition as the core without the TFM. The TFM is assumed to be homogeneously and uniformly distributed throughout the core volume. Most noteworthy is the finding that the minimum over-moderated critical mass of fissile uranium in saturated granite having 30% porosity is 35 kg of ^{235}U.

The minimum over-moderated (by which we actually mean that is not under-moderated) critical mass is significantly larger than the absolutely minimum critical mass. The minimum critical mass (of both kinds) is sensitive to a couple of the medium characteristics—porosity (saturation is assumed) and rock composition. The higher the porosity and the closer the medium's nuclear properties are to those of SiO_2, the smaller will be the minimum critical mass.

Critical systems made by homogeneous deposition of U(12) in saturated rock will have negative reactivity feedback due to either uranium temperature increase (Doppler broadening) or rock temperature increase (spectrum hardening). Hence, due to overmoderation, homogeneous U(12) critical systems can not be autocatalytic beyond a small initial power excursion. However, critical systems made by heterogeneous deposition of U(12) in saturated granite and silica can be autocatalytic, as the combined reactivity effect of uranium and rock temperature increase can be positive. In order for the temperature feedback to be positive, the uranium deposition layer must be thicker than the equivalent of 0.2 mm U(12)O_2 at 10.96 g/cm^3. Mixing of the U(12) with the rock provides another positive reactivity feedback mechanism.

Table 4.5 Summary of Minimum Critical ^{235}U Masses [kg] / Core Radii [cm] for Homogeneous, Spherical, Reflected U(12)O_2 + Rock + H_2O Systems

Medium / Porosity	Minimum critical mass [kg] /Core radius [cm]	
	Absolute minimum	Minimum over-moderated
Water	1.5 / 19	—
SiO_2 / 10%	17 / 71	48 / 130
Granite / 10%	60 / 90	infinite
Granite /30%	7.0 / 37	35/90

Based on basic neutron physics considerations and on the findings of the previous study [1,2] we expect the critical mass in heterogeneous systems to be larger than in the corresponding homogeneous systems. The scope of the present work was too limited to enable us to quantify the minimum critical mass of heterogeneous systems of U(12), and to calculate the magnitude, in these systems, of the various reactivity feedback mechanisms.

Recommended future undertakings include the study of heterogeneous depositions of U(12) in finite cores. The study should pay special attention to the highest plausible porosity (the largest porosity considered in the present study was 30%). If the water to be found in the repository were certain to be saline, the minimum plausible salinity level should be considered for the criticality analysis (we assumed fresh water, thus getting the lower bound on the minimum critical mass). In addition, it appears desirable to identify that level of uranium enrichment which will make the minimum over-moderated critical mass, in granite having the maximum conceivable porosity, too large to be of concern. With this information, it will be possible to evaluate the feasibility of designing the HLW canister in a way that will limit the maximum enrichment level of the deposited uranium to below the level of concern for criticality accidents. One design approach in mind is to add some depleted uranium to the canister.

5. CONCLUSIONS AND FUTURE WORK

For weapons-grade plutonium and highly-enriched uranium disposed of at Yucca Mountain proposed repository [2-4], it has been found that there exists positive reactivity feedback with fissile energy release. An independent assessment of the feasibility of autocatalytic criticality in the case of HLW has been performed in this study for a hypothetical repository in water-saturated granitic rock.

Although TFM content in each waste canister is small, ^{235}U enrichment can be higher than for the case with spent fuel without reprocessing. This is because the mass of minor actinides, which eventually decay to uranium, becomes relatively important in comparison with the mass of uranium initially in HLW glass logs. By radionuclide transport analysis, we have estimated the mass of uranium accumulation and its enrichment. Accumulation is assumed to occur in the host rock away from, and contributed by, 40,000 HLW canisters in the repository. This analysis has been done in such a way that it gives an upper bound of the mass of accumulated uranium and its enrichment.

We have found the possibility that a significant amount of uranium deposition would occur if uranium has a greater solubility and smaller sorption distribution coefficients with the host rock, than its precursing radionuclides. Due to the long half-lives of ^{235}U and ^{238}U, a single failed canister, which is 1000 m from the accumulation location, can supply about 1 mol of uranium with 12% ^{235}U enrichment.

Since we identified the possibility of accumulation of 12% enriched uranium, we have investigated the mass of accumulated 12% enriched uranium required for overmoderated criticality in granite.

The mass of 12% enriched uranium required to make an overmoderated critical system in saturated granite of 10% or lower porosity appears to be too large to be of concern. However, if the rock porosity is 30% or greater, then the formation of the overmoderated critical mass cannot be ruled out.

We have conducted an analysis for positive feedback mechanisms. Possible positive feedback mechanisms in geologic formations for highly enriched TFMs have already been pointed out in [2-4]. We have considered whether the same positive feedback mechanisms are also possible for the 12%-enriched uranium accumulation.

While homogeneous 12%-enriched uranium critical systems can not be autocatalytic beyond a small initial power excursion, due to overmoderation, critical systems made by heterogeneous deposition of 12%-enriched uranium in saturated medium can be autocatalytic, as the combined reactivity effect of uranium and rock temperature increase can be positive. Mixing of deposited uranium with the rock provides another positive reactivity feedback mechanism.

Thus, starting with the 40,000 vitrified HLW waste glass logs placed in water-saturated geologic formations, we can conceive scenarios which lead to supercritical systems that exhibit positive reactivity feedback mechanisms.

The next question would be the likelihood of such scenarios. In the present analysis for transport and accumulation of TFM in the host rock, we have found that significant accumulation could occur only if uranium has a greater solubility and smaller sorption distribution coefficients than the precursors. From the neutronics analysis, we found that if the porosity of the host rock is greater than 30%, the likelihood for overmoderated criticality cannot be ignored. Although we postulate that the likelihood might be very low, considering the very conservative assumptions we made in the analysis, we need to know more about the geochemical and geological conditions of the host rock to quantify the likelihood.

Further studies are recommended for the following aspects in order to decrease extreme conservativeness from the results obtained in this study:

- Development of a more realistic transport model, by taking into account more detailed descriptions on geochemical and hydrological processes, such as radionuclide dispersion during the transport through the host rock due to fracture network and other heterogeneities in the rock and the mechanisms of uranium depositions including precipitation,
- More detailed neutronics analysis for heterogeneous finite systems consisting of 12% enriched uranium, rock, and water, and effect of rock porosity (up to 50%), and
- Uncertainty analysis by taking into account the variations of parameter values.

With engineering measures, or with appropriate criteria for repository siting and design, the likelihood for the autocatalytic criticality could be decreased. Such measures include

- Adding depleted uranium obtained from the tail of the uranium enrichment plant. Then, the uranium deposition will be diluted with more ^{238}U, and the minimum critical mass can be made unrealistically large,
- Removing americium from HLW before the latter is vitrified. Then, the ^{235}U enrichment can be made low enough for supercriticality,
- Recovering uranium at the reprocessing stage at a lower recovery ratio (thus retaining more uranium in the glass log), and
- Selecting a host rock which does not contain regions of porosity greater than 30% within 1000 m from the repository. (The distance between the repository and the high-porosity regions is determined in relation with the solubility and sorption retardation coefficients of uranium.)

We also recommend that, since the possibility of the autocatalytic criticality event has been pointed out for the vitrified HLW disposal, the criticality analysis should be added as an item of the safety assessment for the future geologic repository for HLW.

6. REFERENCES

[1] C. D. Bowman, and F. Venneri, *Underground Autocatalytic Criticality from Plutonium and Other Fissile Material*, Los Alamos National Laboratory, LA-UR-94-4022A, March (1995).

[2] W. E. Kastenberg, P. F. Peterson, J. Ahn, J. Burch, G. Casher, P. L. Chambré, E. Greenspan, D. R. Olander, J. Vujic, B. Bessinger, N. G. W. Cook, F. M. Doyle, and B. Hilbert, *Mechanisms for Autocatalytic Criticality of Fissile Materials in Geologic Repositories*, UCB-NE-4214 (1996).

[3] W. E. Kastenberg, P. F. Peterson, J. Ahn, J. Burch, G. Casher, P. L. Chambré, E. Greenspan, D. R. Olander, J. Vujic, B. Bessinger, N. G. W. Cook, F. M. Doyle, and B. Hilbert, Consideration of Autocatalytic Criticality of Fissile Materials in Geologic Repositories, *Nuclear Technology*, **115**, 298–310 (1996).

[4] W. E. Kastenberg, P. F. Peterson, J. Ahn, J. Burch, G. Casher, P. L. Chambré, E. Greenspan, D. R. Olander, J. Vujic, B. Bessinger, N. G. W. Cook, F. M. Doyle, and B. Hilbert, Scenario Assessment of Autocatalytic Criticality in the Yucca Mountain Geologic Repository, *Waste Management 97*, Tucson, Arizona, March 2–6, 1997 (1997).

[5] Power Reactor and Nuclear Fuel Development Corporation, *Technical Report on Research and Development for Geological Disposal of High-Level Radioactive Wastes*, PNC TN 1410 92-08 (1992).

[6] NAGRA, *Kristallin-I: Safety Assessment Report*, Tech. Rep. 93-22E, NAGRA, Wettingen, Switzerland (1994).

[7] G. H. Canavan, *et al.*, *Comments on 'Nuclear Excursions' and 'Criticality Issues'*, Los Alamos National Laboratory, LA-UR-95-0851, March 7 (1995).

[8] P. B. Parks, M. L. Hyder, T. G. Williamson, *Final Issue of 'Consequences of the Bowman-Venneri Nuclear Excursion Thesis on the Prospects for Placing Vitrified Plutonium Canisters in Geologic Repositories' (U)*, Westinghouse Savannah River Company, PDI-SPP-95-0023, June 5 (1995).

[9] R. A. Van Konynenburg, *Comments on the Draft Paper 'Underground Supercriticality for Plutonium and Other Fissile Material'*, Lawrence Livermore National Laboratory, UCRL-ID-120990 COM, May 5 (1995).

[10] M. J. Bell, *NRC Comments on the Report 'Underground Supercriticality From Plutonium and Other Fissile Material'*, U.S. Nuclear Regulatory Commission, August 7 (1995).

[11] G. A. Cowan, A Natural Fission Reactor, *Scientific American*, **235**, 36 (1976).

[12] E. D. Clayton, *Anomalies of Nuclear Criticality*, Pacific Northwest Laboratory, Richland, WA, PNL-SA-4868 Rev. 5, June (1979).

[13] B. F. Gore, U. P. Jenquin, R. J. Serne, *Factors Affecting Criticality for Spent-Fuel Materials in a Geologic Setting*, Pacific Northwest Laboratory, PNL-3791, April (1981).

[14] F. J. Dahlkamp, Uranium Ore Deposits, Springer-Verlag, Berlin (1991).

[15] M. Benedict, T. H. Pigford, H. W. Levi, *Nuclear Chemical Engineering*, 2nd Ed., McGraw-Hill, 1981.

[16] A. G. Croff, *A User's Manual for the ORIGEN 2 Computer Code*, ORNL/TM-7175, Oak Ridge national Laboratory (1980).

[17] R. Sanchez, *et al.*, *Criticality Characteristics of Mixtures of Plutonium, Silicon Dioxide, Nevada Tuff, and Water*, Los Alamos National Laboratory, LA-UR-95-2130, (1995).

[18] *Chigaku Jiten* (Geology Encyclopedia), Heibon-Sha, Tokyo (1981).

[19] J. J. Duderstadt and L. J. Hamilton, *Nuclear Reactor Analysis*, John Wiley & Sons, New York (1976).

[20] D. P. Hodgekinson and P. R. Maul, 1-D Modelling of Radionuclide Migration Through Permeable and Fractured Rock for Arbitrary Length Decay Chains Using Numerical Inversion of Laplace Transforms, *Ann. Nucl. Energy*, **15**(4), 175-189 (1988).

[21] D. H. Tang, E. A. Sudicky and E. O. Frind, Contaminant Transport in Fractured Porous Media: Analytical Solution for a Single Fracture, *Water Resources Research*, **17**, 555–564 (1981).

[22] P. L. Chambré, T. H. Pigford, W. W.-L. Lee, J. Ahn, S. Kajiwara, C. L. Kim, H. Kimura, H. Lung, W. J. Williams, and S. J. Zavoshy, *Mass Transfer and Transport in a Geologic Environment*, Lawrence Berkeley Lab., LBL-19430 (1985).

[23] J. Ahn and A. Suzuki, Diffusion of the ^{241}Am —> ^{237}Np Decay Chain Limited by Their Elemental Solubilities in the Artificial Barriers of High-Level Radioactive Waste Repositories, *Nuclear Technology*, **101**, 79--91 (1993).

[24] J. Ahn, T. Ikeda, T. Ohe, T. Kanno, Y. Sakamoto, T. Chiba, M. Tsukamoto, S. Nakayama, S. Nagasaki, K. Banno, and T. Fujita, Quantitative Performance Allocation of Multi-Barrier System for High-Level Radioactive Waste Disposal, *Journal of Atomic Energy Society of Japan*, **37**(1), 59-77 (1995).

[25] H. Sato, T. Ishimaru, H. Sugihara, and K. Shimizu, *Data for Mechanical Properties of Japanese Rock, Literature Survey*, PNC TN 7410 92-018 (1992).

[26] H. Sato, T. Ashida, Y. Obara, M. Yui, H. Umeki, and K. Ishiguro, *Effective diffusion Coefficients for Radionuclides in Bentonite and in Rocks*, PNC TN 8410 92-164 (1992).

[27] M. Kurohane, T. Ashida, T. Shibuya, S. Inui, M. Okazaki, and M. Yui, Pu Dissolution from Pu-doped glass, H73, *Proc. Fall Mtg. Atom. Energy Soc. Japan*, (1995).

[28] D. Rai, A. R. Felmy, J. L. Ryan, Uranium (IV) Hydrolysis Constants and Solubility Product of $UO_2 \cdot xH_2O$ (am), *Inorg. Chem.*, **29**, 260-264, (1990).

[29] T. Shibuya, H. Yoshikawa, H. Sato, M. Yui, H. Umeki, and K. Ishiguro, *Sorption Distribution Coefficient of Radionuclides in Bentonite and in Rocks*, PNC TN 8410 92-163, (1992).

[30] G. M. N. Baston, J. A. Berry, M. Brownsword, M. M. Cowper, T. G. Heath, and C. J. Tweed, The Sorption of Uranium and Technetium on Bentonite, Tuff and Granodiorite, S*ci. Basis Nuc. Was. Man., XVIII*, 989-996, (1995).

[31] IMSL, Math Library, FORTRAN Subroutines for mathematical Applications, IMSL Inc., Houston, Texas.

[32] A. Talbot, The Accurate Numerical Inversion of Laplace Transforms, *J. Inst. Math. Applic.*, **23**, 97-120 (1979).

[33] J. A. Barker, Laplace Transform Solutions for Solute Transport in Fissured Aquifers, *Adv. Water Resources*, **5**, 98 (1982).

[34] L. C. Sanchez *et al*., "Critical Modeling," Chapter 10 in R. P. Rechard, Editor, "Performance Assessment of the Direct Disposal in Unsaturated Tuff of Spent Nuclear Fuel and High-Level Waste Owned by U.S. Department of Energy," Sandia National Laboratory Report SAND94-2563 (1995).

[35] D. K. Parsons *et al*., "Los Alamos Review of the Bowman-Venneri Paper Regarding Possible Underground Criticality," Los Alamos National Laboratory Internal Report LA-UR 95-2152 (Presented to the "Special ANS Panel: Criticality Stability of Fissile Material Underground," at the ANS Annual Meeting, Philadelphia, PA June 24-29, 1995.

[36] J. F. Briesmeister, "MCNP - A General Monte Carlo N-Particle Transport Code, Version 4A," Los Alamos National Laboratory, Los Alamos National Laboratory Report LA-12625 (1993).

[37] H.C. Paxton and N.L. Pruvost, "Critical Dimensions of Systems Containing ^{235}U, ^{239}Pu and ^{233}U," Los Alamos National Laboratory Report LA-10860-MS (1987).